



저작자표시-비영리-변경금지 2.0 대한민국

이용자는 아래의 조건을 따르는 경우에 한하여 자유롭게

- 이 저작물을 복제, 배포, 전송, 전시, 공연 및 방송할 수 있습니다.

다음과 같은 조건을 따라야 합니다:



저작자표시. 귀하는 원저작자를 표시하여야 합니다.



비영리. 귀하는 이 저작물을 영리 목적으로 이용할 수 없습니다.



변경금지. 귀하는 이 저작물을 개작, 변형 또는 가공할 수 없습니다.

- 귀하는, 이 저작물의 재이용이나 배포의 경우, 이 저작물에 적용된 이용허락조건을 명확하게 나타내어야 합니다.
- 저작권자로부터 별도의 허가를 받으면 이러한 조건들은 적용되지 않습니다.

저작권법에 따른 이용자의 권리는 위의 내용에 의하여 영향을 받지 않습니다.

이것은 [이용허락규약\(Legal Code\)](#)을 이해하기 쉽게 요약한 것입니다.

[Disclaimer](#)

Master's Thesis of M.S

Sulfur Isotope Geochemistry of Ice Wedges, Northeastern Siberia

황 동위원소를 이용한 동시베리아 얼음썰기의
지화학 연구

August 2023

Graduate School of Natural Sciences
Seoul National University
Earth and Environmental Sciences Major

Hyeonjeong Jeong

Sulfur Isotope Geochemistry of Ice Wedges, Northeastern Siberia

Advisor Min Sub Sim

Submitting a master's thesis of
Science in Earth and Environmental Sciences

May 2023

Graduate School of Natural Sciences
Seoul National University
Earth and Environmental Sciences Major

Hyeonjeong Jeong

Confirming the master's thesis written by

Hyeonjeong Jeong

July 2023

Chair _____ (Seal)

Vice Chair _____ (Seal)

Examiner _____ (Seal)

Abstract

With its unique stable isotope ratio and involvement in various biogeochemical processes, sulfur serves as a valuable paleoenvironmental proxy. Ice wedges have recently been evaluated as archives for aerosols, precipitation, and organic matter, serving as useful archives of paleoenvironmental information. However, sulfur isotopic compositions in ice wedges have not yet been comprehensively explored or understood. This study presents the first sulfur isotope geochemical data from the ice wedge of Northeastern Siberia. The samples were collected from the Yakutsk (Cyuié, Churapcha, Syrdakh), Zyryanka, and Batagay regions and separated into dissolved sulfate, particulate organic matter (POM), and lithic particles. The sulfur isotopic composition from the different areas shows consistent trends in each component. Yakutsk showed significant enrichment of more than 6‰ compared to the other study regions. Despite their distance, Cyuié, Churapcha, and Syrdakh in the Yakutsk region have similar sulfur isotopic compositions but are differed from values from the Zyryanka and Batagay regions. This observation suggests a potential influence of the local bedrock on sulfur sources. Sulfur isotopic compositions between modern precipitation, plant sulfur, and ice wedges in Yakutsk and the upper and lower Batagay sections could not find temporal variations in sulfur isotopic composition. Instead, the differences observed within the same ice wedge suggest that while the source of sulfur-containing materials remains consistent, the ice wedge may have temporal sensitivity to glaciation. In-house freezing experiments and sulfide assay in the ice wedge found that there was no fractionation during the freezing process and by

sulfate-reducing microorganisms within the ice wedge, indicating that the sulfur contained in the ice wedge preserves the isotopic composition of the source material. This study establishes an experimental method for analyzing sulfur isotope analysis in ice wedges and is the first to use sulfur isotope composition data to interpret the paleoenvironment of northeastern Siberia. The sulfur isotopic composition data suggests that sulfur isotopic composition has the potential to serve as a proxy, reflecting the geochemistry of the surrounding environment at the time of ice wedge formation, and bedrock is the possible factor on sulfur isotopic composition in ice wedges from inland. Furthermore, the observed spatial variation in sulfur isotopic composition within the ice wedge is anticipated to offer insights into the temporal evolution of the ice wedge over time, with the potential advancement of future high-resolution dating techniques. These findings are essential for further understanding past ice wedge formation environments and provide a new method to explore the history of ice wedges.

Keyword : Sulfur isotope, Ice wedge, Paleoenvironmental proxy, Pyrite weathering, Northeastern Siberia

Student Number : 2021-27813

Table of Contents

List of Tables	iv
List of Figures	v
1. Introduction	1
2. Study sites and ice wedge samples	5
3. Methods	10
3.1 Sample pretreatment	10
3.2 Sulfur extraction from POM, Lithic particles.....	11
3.3 Quantification and sulfur isotope analysis.....	13
3.4 In-house freezing experiment	15
4. Results	18
5. Discussion	29
5.1 Factors controlling the Ice wedge sulfur geochemistry.....	29
5.1.1 Dissolved sulfate	29
5.1.2 POM	33
5.1.2 Lithic particle.....	35
5.2 Temporal variation $\delta^{34}\text{S}$ in ice wedge.....	36
6. Conclusion	41
References	44
Abstract in Korean	54

List of Tables

Table 1. Instrument operating conditions for S isotope determination using MC-ICP-MS.....	16
Table 2. Geochemistry data from the northeastern Siberia	21
Table 3. Sulfur concentration and isotopic composition data from in-house freezing experiment	23
Table 4. Sea salt contributions of sulfate in ice wedge.....	39

List of Figures

Figure 1. The natural range of $\delta^{34}\text{S}$ values of Earth.....	4
Figure 2. Map of study area.....	8
Figure 3. Overview of ice wedge outcrop.....	9
Figure 4. Overall ice wedge sample treatment flow chart for sulfur isotope analysis.....	17
Figure 5. Sulfur isotope values in the ice wedges from the northeastern Siberia used in the study.	24
Figure 6. Sulfate concentration and isotope composition of dissolved sulfate in the study area	25
Figure 7. Sulfate concentration and $\delta^{34}\text{S}_{\text{SO}_4}$ within the ice wedge from Zyryanka B site.....	26
Figure 8. SEM image and EDS elemental spectrum of handpicked sample from B19-IW3 mineral particle.....	27
Figure 9. In-house freezing experiment data to evaluate the potential fractionation of $\delta^{34}\text{S}_{\text{SO}_4}$.....	28
Figure 10. Correlation between $\delta^{34}\text{S}_{\text{SO}_4}$ and $\delta^{34}\text{S}_{\text{POM}}$.....	40

보존용 학위논문 정오표

페이지	정정 전	정정 후
p. 5 : 9	Pop	Popp
p. 6 : 3	Péwé & Journaux, 1983	Péwé & Journaux, 1983
p. 7 : 7, 20	Yang et al., 2022	Yang et al., 2023
p. 7 : 20	Park et al., 2021	Park et al., 2022
p. 9 : 3	Yang et al., 2022	Yang et al., 2023
p. 9 : 6	Ko et al., 2020	Ko, 2023
p. 12 : 13	RCP	RCF
p. 13 : 11	AS10	AG10
p. 14 : 22	SBB	SSB
p. 19 : 3	1.0	0.7
	6.8	8.3
	-1,5‰	-1.5‰
p. 28 (Figure 9)	Frozen	Frozen
p. 30 : 1	Guo et al., 2009	Guo et al., 2010
p. 32 : 11	Pewe et al., 1983	Péwé & Journaux, 1983
p. 34 : 18	Shepelev et al., 2018	Shepelev et al., 2020
p. 44 - (References)	<p>Ko, J. (2009). Petroleum Geology of the East Siberian Platform, Russia. <i>Journal of the Korean Society of Mineral and Energy Resources Engineers</i>, 46(6), 809-833.</p> <p>Ko, N., Yang, J.-W., Iwahana, G., Fedorov, A., Shepelev, A. G. <i>et al.</i> (2021). Paleoclimate Inferred from Concentration of Greenhouse Gas and Ratios of O₂/Ar and N₂/Ar in Ice Wedges in Northeastern Siberia and Northern Alaska. EGU General Assembly Conference Abstracts,</p> <p>Meyer, H., Schirrneister, L., Andreev, A., Wagner, D., Hubberten, H.-W. <i>et al.</i> (2010). Lateglacial and Holocene isotopic and environmental history of northern coastal Alaska—Results from a buried ice-wedge system at Barrow. <i>Quaternary Science Reviews</i>, 29(27-28), 3720-3735.</p> <p>Meyer, H., Schirrneister, L., Yoshikawa, K., Opel, T., Wetterich, S. <i>et al.</i> (2010). Permafrost evidence for severe winter cooling during the Younger Dryas in northern Alaska. <i>Geophysical Research Letters</i>, 37(3).</p> <p>Vasil'chuk, Y. K.&Vasil'chuk, J. Y. (2019). The first AMS dating of organic microinclusions in an ice wedge of the upper part of the Batagay yedoma megaslump (Yakutia). <i>Doklady Earth Sciences</i>,_</p> <p>Vinogradov, V., Pokrovskiy, B., Pustynnikov, A., Muravyev, V., Shatskiy, G. <i>et al.</i> (1994). Isotopno-geokhimicheskie osobennosti i vozrast verkhnedokembriyskikh otlozheniy zapada Sibirskoy platformy. <i>Litol. Polezn. Iskop</i>, 4, 49-76.'</p>	<p>* These papers are not relevant to this study, and the papers below should be added for reference.</p> <p>Jongejans, LL., Mangelsdorf, K., Karger, C., Opel, T., Wetterich, S. <i>et al.</i> (2022). Molecular biomarkers in Batagay megaslump 629 permafrost deposits reveal clear differences in organic matter preservation between glacial and 630 interglacial periods. <i>The Cryosphere</i>, 16(9), 3601-3617.</p> <p>Nriagu, J., Rees, C.E., Mekhtieva, V.L., Lein, A.Y., Fritz, P. <i>et al.</i> (1991). Hydrosphere. In: Krouse, H.R., Grinenko, V.A. (Eds.), <i>Stable Isotopes in the Assessment of Natural and Anthropogenic Sulfur in the Environment</i>. John Wiley & Sons Environment, Chichester, pp. 177-265.</p> <p>Park H. (2023). <i>Biogeochemical studies of greenhouse gas formation from two ice complexes of Batagay Megaslump, East Siberia</i> University of Seoul (Korea).</p> <p>Vinogradov, A.P. & Grinenko, L.N. (1966). The isotopic composition of sulfur of sulfides in Cu-Ni deposits and ore occurrences in the Norilsk district in connection with their genesis. <i>Geokhimiya</i>, 1, 3-14</p>

1. Introduction

Ice wedges are a type of ground ice found in permafrost and widely distributed throughout the Northern Hemisphere (Alaska, northern Canada, and Siberia). These ices are characterized by vertically developed foliation and varying sizes of wedge-shaped bodies located beneath the polygonal patterns in permafrost (Leffingwell, 1915; Harry & Gozdzik, 1988). The growth of ice wedges occurs due to repeated frost-cracking and crack infilling. During winter, thermal contraction causes the frozen ground, including the active layer, to crack vertically, and multiple sources can fill these cracks, including (a) spring or summer meltwater derived from snow, (b) winter snow and/or hoarfrost, and (c) windblown mineral, soil, or organic material (Leffingwell, 1915; Soare et al., 2014; Opel et al., 2018). Meltwater quickly refreezes at subzero temperatures and forms vertical ice veins to grow, extending up to 10 m in width over hundreds to thousands of years (Opel et al., 2018). In general, thermal contraction cracks tend to form at the center of the last-formed ice vein, and then the ice wedge has a structure older from the center toward the edges as repeated processes. However, ice wedges in nature have a more intricate and unpredictable structure.

During the formation of cracks and refilling, various materials indicating the environment or climate can become trapped within the veins. If the ice wedge has not experienced melting since its formation, it can be used as an archive, preserving a record of past climate and environment. As an archive, the main advantage of ice wedges is the extensive occurrence of ice wedges within the permafrost. Ice cores, traditionally used in paleoclimate studies, are spatially

limited mainly to Antarctica, with only a few in Greenland and Canada. Thus, ice wedges can be a helpful tool for understanding the paleoclimate of the Northern Hemisphere. Ice wedges also reflect winter conditions, which may help bridge the gap with other biological proxy data (e.g., diatoms, tree rings) that reflect summer temperatures. Based on these advantages, recent studies have increasingly recognized the significance of ice wedges as valuable proxies in paleoclimate and paleoenvironmental reconstruction. For instance, water isotope records have been used to confirm the Holocene winter warming trend (Opel et al., 2011; Meyer et al., 2015; Opel et al., 2017), carbon isotope and biomarkers in soil have been inferred environmental change in ice wedges (Vasil'chuck et al., 2020). The study of ice wedges has been proven useful in previous work to characterize past climate and environment as well as trace shoreline change (Iizuka et al., 2019; Holland et al., 2023). However, studies have yet to attempt to reconstruct the paleoenvironment of ice wedges using sulfur isotope as a proxy.

Sulfur has characteristic isotope signatures (Figure 1) produced by chemical or biological reaction cycling between different environmental spheres. Most of the sulfur is stored in surface rocks, and sulfur-bearing minerals such as anhydrite, gypsum, barite, and pyrite can exhibit highly variable sulfur isotope ratio ($\delta^{34}\text{S}$) with a range of -40 to +40‰ (Thode, 1991) depending on their origin. The majority of $\delta^{34}\text{S}$ values were observed to form clusters around 0‰ (igneous, volcanic, or meteoric origin) and +20‰ (evaporites). The reflection of the different microbial activities, sedimentary pyrite has some extreme endmembers. In aquatic environments, modern oceans, the average sulfur isotope ratio is +20.3‰, while with $\delta^{34}\text{S}$ values for rain, snow, and freshwater sources ranging from 0 to +10‰

(Nriagu et al., 1991). Organic sulfur exhibits differing isotopic values depending on originated sources. Sulfur from marine sources shows higher values (+15‰ to +19‰; Oduro et al., 2012), while terrestrial biogenic emissions yield lighter values (-10‰ to -2‰; Panettiere et al., 2000; Zhang et al., 2010; Xiao et al., 2011). Thus, comprehending the $\delta^{34}\text{S}$ values in nature is essential for reconstructing paleoenvironments as it provides insight into the origin of sulfur-containing materials and contributions of microbial metabolic processes in controlling the sulfur cycle.

The objective of this study is to propose sulfur isotopes as novel potential proxies for paleoenvironment and paleoclimate in ice wedges. To achieve this aim, ice samples Yakutsk (Cyuie, Churapcha, Syrdakh), Zyryanka, and Batagay in northeastern Siberia, Russia, were separated into dissolved sulfate, organic matter, and lithic particles to analyze sulfur isotopic composition. The results of the samples were categorized by region, enabling a comparison of the differences, and identified factors characteristic of each site where the samples were collected, assessing their influence on the enclosing materials. Furthermore, by conducting an in-house freezing experiment and sulfide assay, the potential of in situ fractionation of sulfur was tested, and the ice wedge itself can serve as an archive for sulfur isotopic values. This research may show the most effective sulfur sources for ice wedges growing inland and provide new insights into the paleoenvironment/climate by expanding the application of ice wedges as well as implications for ice wedge paleoclimate interpretations.

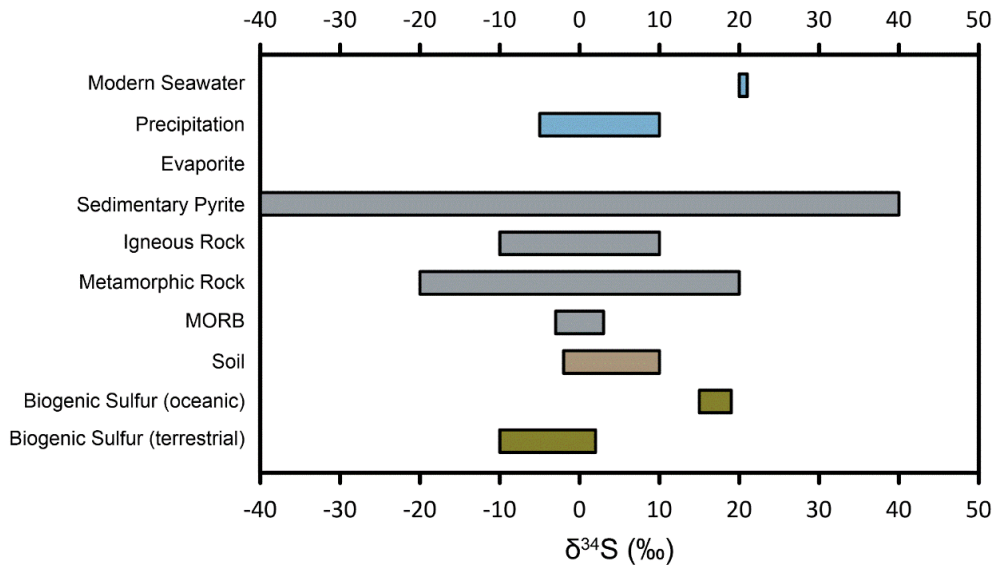


Figure 1. The natural range of $\delta^{34}\text{S}$ values of Earth (Thode, 1991; Hannan, 1998; Panettiere et al., 2000; Zhang et al., 2010; Xiao et al., 2011; Oduro et al., 2012; Nehlich, 2015; Hammerli et al., 2021).

2. Study sites and ice wedge samples

Ice wedge samples were collected from three sites in northeastern Siberia: Yakutsk (Cyui, Churapcha, Syrdakh), Zyryanka, and Batagay (Figure 2). Northeastern Siberia comprises a diverse geological setting comprising terrestrial collisional belts and cratons, each characterized by distinct stratigraphic and lithological features (Figure 2). This study area specifically lies within the confines of the Siberian Craton, a prominent stable region, and the Verkhoyansk-Kolyma orogen, an orogenic belt known for its tectonic complexities and geological significance (Pop et al., 2006). The collision of rocks from different origins in this region results in a distinctive transition from marine carbonates and evaporites to terrestrial clastic marine and continental environments (Steiner & Barnet, 2021). The climate of Northeastern Siberia is characterized by a typical continental subarctic climate, with mean temperatures of -40°C and 16.2°C for January and July, respectively (Gidrometeoizdat, 1989; Kim et al., 2019; Murton et al., 2022). The active layer thickness in the region varies from 0.4 to 1.2 meters, contingent on soil and vegetation types (Ivanova, 2003). However, in Yakutsk, the active layer thickness is notably thicker, ranging from 1.2 to 2.5 meters, due to its relatively higher summer temperatures, reaching 19.5°C in July (Fedorov & Konstantinov, 2003). The region experiences low annual precipitation, approximately 200 mm, with the majority falling as summer rain.

Ice wedge samples were collected from Cyui: in the 2015 summer, Churapcha: in the 2016 autumn, Syrdakh: in the 2015 summer, Zyryanka: in the 2017 summer, and Batagay: in the 2017 summer (Kim et al., 2019; Opel et al.,

2019; Yang et al., 2020; Ko, 2023; Yang et al., 2023) (Figure 3). Yakutsk lies in the central Yakutia lowland, which is covered with a well-sorted uniform tan loess-like silt in variable thicknesses between 0.5 and 30 m (Péwé & Journaux, 1983). Three sites, Cyuie, Churapcha, and Syrdakh, near Yakutsk, are all located within 150 km of each other. The Cyuie site is located approximately 30 km southeast of Yakutsk (61.73°N, 130.42°E). Samples were collected from two outcrops at the Cyuie site, but only samples from the CYB outcrop were utilized in this study. The Churapcha site is located 180 km from the east of Yakutsk (61.97°N, 132.61°E), and the Syrdakh site is located 100 km northeast of Yakutsk on the Tyunglunskiy terrace of the Lena River (62.33°N, 130.58°E). Both sampling sites were situated near a thermokarst lake where lateral thermal erosion was active. Zyryanka is located in the Kolyma Basin southern boreal region of the Kolyma River, which is affected by thermokarst development. The region is underlain by Holocene alluvial and Pleistocene lacustrine-alluvial deposits. Ice samples were used from two sites (A, B site) in Zyryanka (65.93°N, 150.89°E). Ice wedge of Zyryanka, site A block samples were taken horizontally at a depth of about 2.5 m from the ground, and site B block samples were collected horizontally from the lower portion of the ice wedge exposure. In Zyryanka ice wedges, samples were collected from two distinct types: pure ice wedge samples and samples formed by refrozen soil water, which consists of various natural waters and contains considerable soil sourced adjacent permafrost soil. The Batagay Megaslump (67.58°N, 134.77°E), situated around 10 km southeast of Batagay in Yakutia, exposes four significant chronostratigraphic units located above the underlying slate bedrock (Kunitsky et al., 2013; Opel et al., 2019; Murton et al., 2022), and samples were taken from two extensive ice wedges

known as the upper and lower ice complex.

The age dating results by radiocarbon (^{14}C) decay analysis show that the Yakutsk ice wedges were formed during the Last Glacial Maximum (LGM). The ages of the Cyuie ice wedges were determined to be between $18,130 \pm 190$ and $19,270 \pm 360$ years BP from ^{14}C dating of CO_2 gas. The Syrdakh and Churapcha ice wedges were likely formed between $20,970 \pm 80$ and $26,570 \pm 160$ years BP (Yang et al., 2022). The age of plant remains in the Cyuie host sediments of $27,140 \pm 150$ years BP (Kim et al., 2019). The ^{14}C ages of Zyryanka samples are from 810 to 1,750 BP, corresponding to the late Holocene (Ko et al., 2022). From the Batagay upper ice complex, plant material resulted in a date of 22 ± 60 ka to 49 ± 580 ka BP corresponding to the late Holocene (Ashastina et al., 2017; Murton et al., 2017; Opel et al., 2019; Vasil'chuk et al., 2022). In the lower ice complex, the results of post-infrared infrared-stimulated luminescence (pIRIR) dating of K-feldspar from sand estimated that the ice wedge developed at least 650 ka in the middle Pleistocene (Murton et al., 2022). $\delta(\text{N}_2/\text{Ar})$ of ice wedge gas, which can mean whether snowmelt occurred during the formation of the ice wedges, indicates that the ice wedges from Yakutsk and Batagay were formed by dry snow compaction rather than snowmelt infilling into the frost cracks. Meanwhile, the Zyryanka ice wedges were formed by liquid water and dry snow (Kim et al., 2019; Park et al., 2021; Ko et al., 2022; Yang et al., 2022).

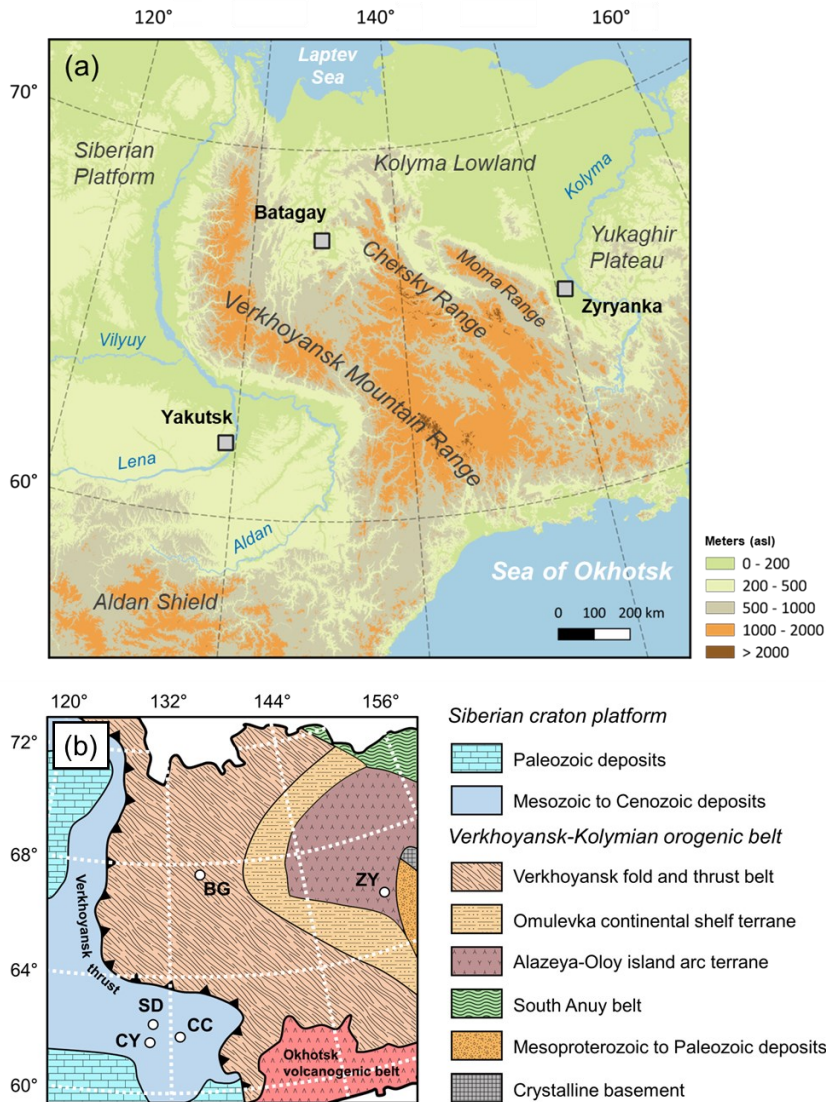


Figure 2. Map of study area. (a) Map showing the topographic setting of the northeastern Yakutia, and the area investigated in this paper (Yakutsk, Zyryanka, Batagay) in gray box; (b) Simplified tectonic map, showing location of the Siberian Craton and the Verkhoyansk-Kolymia orogen, with the sampling sites of Cyuie (CY), Churapcha (CC), Syrdakh (SD), Batagay (BG), and Zyryanka (ZY) highlighted within the white circle.

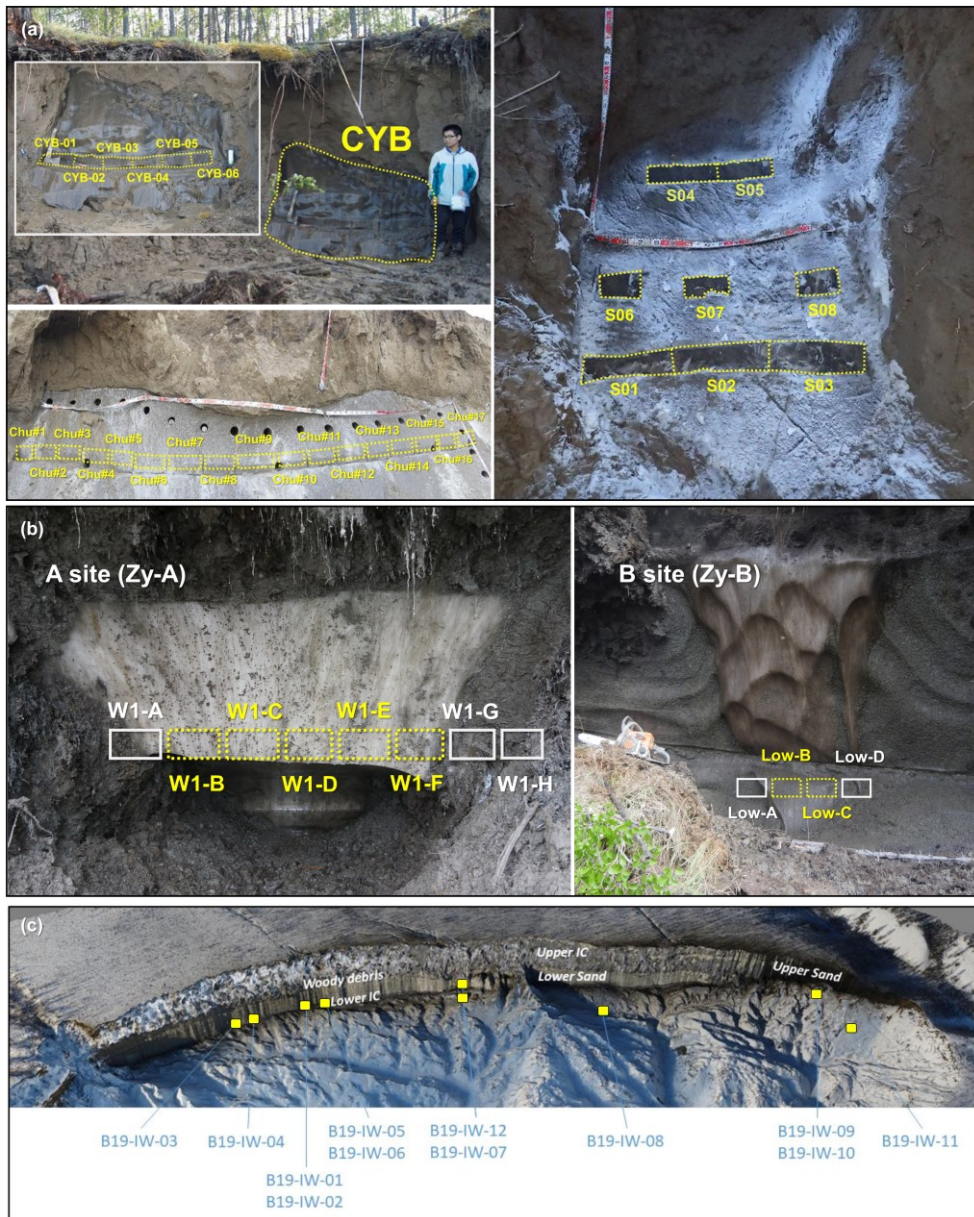


Figure 3. Overall view of ice wedge outcrop. The ice sampling locations are denoted in yellow-dotted lines. (a) Photograph of the Yakutsk ice wedge outcrop. Pictures modified from Yang et al. 2020; 2022. Top left: Photographs of the Cyuie sampling site and detailed pictures of sampling locations. Bottom left: Photographs of the Churapcha sampling site. Right: Photographs of the Syrdakh sampling site. (b) Photograph of the Zyryanka ice wedge outcrop. Pictures modified from Ko et al. 2020. Samples denoted white lines are not pure ice wedge. (c) Photograph of the Batagay megaslump with main stratigraphic units and approximate sampling locations of ice wedges (blue arrows). Pictures modified from fieldwork reports of expedition to Batagay in 2019 (Jongeans et al., 2019).

3. Methods

3.1. Sample pretreatment

In the study, sulfur isotopic compositions of materials comprising the ice wedge – dissolved sulfate, organic matter, and lithic particles were measured to characterize the geochemistry of the ice wedges. The overall process is shown in Figure 4. The ice wedges were cut using a chainsaw into blocks at 100 to 200 g, depending on apparent enclosing sediment contents, and stored in ziplock bags at a -20 °C freezer.

Before proceeding with the sample melting process, it is imperative to thoroughly consider the potential presence of sulfides in the ice, which could lead to alterations in the meltwater's initial sulfur concentration and isotopic composition due to oxidation during thawing. To test this possibility, 0.05 M zinc acetate (ZnAC) solution (ACS reagent, >98%, Sigma Aldrich) was added to a portion of each sample (~10 g). This addition of the ZnAC solution leads to the formation of zinc sulfide (ZnS) through a reaction with the sulfides present, resulting in precipitation. The quantity of Zn^{2+} added was adjusted to achieve a final concentration of 100 μ M in the melted solution, ensuring sulfide the precipitation. Ice samples melted at 4 °C under dark, anaerobic conditions, and then sulfide concentration was assayed by the spectrophotometric method described by Cline (1969). As a result of this assay, the sulfide oxidation effect would be negligible; the remaining samples were melted in the same process without adding the ZnAC solution. After melting, the meltwater and soil were separated by a centrifugal separator (1763 RCF, 10 min). The meltwater was

filtered through a syringe filter (PTFE-H, hydrophilic, 0.2 μm), rinsed three times with deionized water (18 M Ω), and stored at cool conditions for isotope analysis. The wet soil residues were rinsed three times with deionized water and dried at 70 °C for 24 h.

3.2. Sulfur extraction from POM and lithic particles

Organic matter and lithic particles in dried soils were distinguished using heavy liquid separation (Nichols & Wright, 2006) based on the definition of particulate organic matter (POM) in soil science (i.e., <1.8 g/cm³, >63 μm). The fractionation was conducted using a solution of Sodium Metatungstate (H₂Na₆O₄₀W₁₂, Alfa Aesar) as a heavy liquid at a density of 1.75 to 1.85 g/cm³. The heavy liquid was added to 0.5 g of soil in a conical tube (50 ml, Polypropylene, Falcon), and tubes were sonicated and centrifuged (1224 RCF, 30 min) to ensure proper floatation of POM. This procedure was repeated three times. From the floating fractions, POM was collected by sieving through a 63 μm mesh screen. Sinking fractions that represent lithic particles and POM were washed thoroughly three times with deionized water using a centrifugal separator (1763 RCF, 10 min), followed by drying. The heavy liquid used in the experiments could be recycled after filtering with a rinsed bottle top vacuum filter (0.22 μm , Thermo Fisher) and evaporation.

The procedure for sulfur extraction from the POM was followed by Wheal et al. (2011) and Donovan et al. (2016), with modifications based on the sample weight. Dried POM (2-10 mg) samples were placed in a 2 ml microcentrifuge tube (Polypropylene, Simport) with 0.1 ml of HNO₃ (Ultra high purity, 70%, ODLab).

The caps were hand-tightened, and the tubes were vortexed to wet the material perfectly. Then samples were pre-oxidation overnight in a fume hood at room temperature. Initially, the samples were digested at 95 °C for 90 min in a heating block. During digestion, the screw cap should not close completely as the generated pressure may cause the microtubes to rupture, leading to sample loss. The tubes were removed from the heating block and cooled at room temperature before adding 0.1 mL of H₂O₂ solution (for trace analysis, ≥30%, Sigma Aldrich), then re-heated at 95 °C for 30 min. After cooling, 0.1 mL H₂O₂ was added to each sample, followed by a 45 min digestion at 95 °C. If the solution remained not clear or pale yellow, an additional 0.1 ml H₂O₂ was added and heated for 45 min at 95 °C. Following the digestion process, deionized water was added to each tube to the 1 mL mark. The 0.9 ml of supernatants were collected in a Teflon vial by centrifuged (12000 RCP, 3 min) and dried on a graphite heating plate for 12 h. The amounts of HNO₃ and H₂O₂ added during the procedure were adjusted based on the sample quantity. The Teflon vials used in the experiments were washed with deionized water five times, then soaked in 4 M HCl (Reagent grade, SAMCHUN) and heated for a day. After treatment, the vials were rinsed three times with deionized water and dried before use.

Dried lithic particles were homogeneously ground, and 0.5 g of samples were transferred into a 15 ml conical tube. 9 ml of 1N HNO₃ was added to samples and left on the shaker at room temperature for 12 days—all mineral sulfide phases, including pyrite, oxidized to sulfate by this process. After leaching, the supernatant was recovered by centrifugation (1763 RCF, 10 min) and filtered using a syringe filter washed with 1N HNO₃ and deionized water. Around 8.5 ml of recovered

supernatant, 8 ml of this solution was transferred to a Teflon vial, and the solution dried in a graphite heating plate (105 °C, 18 h) (Schimmelmann & Kastner, 1993). Sulfate extracted from POM and lithic particles was dissolved in 0.9 mL of 0.3 M HNO₃ and left on a shaker overnight for complete dissolution. The samples were filtered through a washed syringe filter to remove some solid residues and transferred to a 2 ml microcentrifuge tube.

3.3. Quantification and sulfur isotope analysis

Sulfate concentration was determined by Aquion Ion Chromatography (ICS-1100, Dionex). The ICS-1100 was equipped with an AS-DV automatic sampler, analytical column (Dionex Ionpac AS10-4mm), guard column (Dionex Ionpac AS10-4mm), and a suppressor (Dionex ASRS-4mm). An aqueous solution containing 100 mM NaOH was used for elution. Except for meltwater, the samples were diluted 100 or 500 times because concentrated NO₃⁻ in the solution affects anion separation efficiency. Calibration standards and Na₂SO₄ spike were run during each session to ensure the validity of the calibration curve. The overall error in ion concentration generally falls within the range of 5 to 10%.

Sulfate ions in the sample were separated using AG1-X8 anion exchange resin (100-200 mesh, Chloride form, BIO-RAD). The column (Poly-Prep columns, 0.8 × 4 cm, Bio-Rad) was cleaned with 4 M HCl and filled with 1.4 ml of anion exchange resin. 28 ml 1.6 M HNO₃ (Reagent grade, SAMCHUN), 4 M HCl (Reagent grade, SAMCHUN), and deionized water passed through the column to clean the column. Followed by 14 ml of HCl (Ultra high purity, 70%, ODLab) was added to condition the resin. The amount of sample loaded onto the column was

determined by the final 100 nmol of sulfur. Passed through 28 ml deionized water to remove the cations and recovered in a Teflon container using 8 ml 0.5 M HNO₃ (Ultra high purity, 70%, ODLab). The recovered samples were dried on a graphite heating plate (105 °C, 18 h). Purified samples were dissolved in 0.8 M HNO₃ and diluted to the concentration of the in-house standard (20 μM) using 0.8 M HNO₃. The concentration of Na⁺ in the sample was adjusted to 40 μM using a NaOH solution (IC grade, Sigma-Aldrich) to reduce the effect of the difference in Na⁺ concentration between the standard and the sample for isotope analyses (Paris et al., 2013; Yu et al., 2017).

The sulfur isotopic composition of the prepared samples was analyzed on Nu instruments Multi Collector-Inductively Coupled Plasma Mass Spectrometer (MC-ICP-MS, Plasma 3, UK) installed at the National Center for Inter-university Research Facilities (NCIRF) at Seoul National University. The settings of the instrument were optimized for the day of analysis, and the general conditions of this study are shown in Table 1 (Moon et al., 2021). The sample was introduced to MC-ICP-MS by nebulizer (ESI PFA-100) and desolvator (Cetac Aridus II) to reduce serious interference from molecular ions, mainly hydrogen and oxygen species. Cup configurations for sulfur were H6 cup for ³⁴S, H1 cup for ³³S, and L4 cup for ³²S in medium resolution mode (Resolving power 7000). Sulfur isotope compositions were detected on the interference-free shoulder on the low-mass side of the peak (Craddock et al., 2008; Paris et al., 2013; Moon et al., 2021). Mass bias was corrected using a sample–standard bracketing (SBB) method with repeated measurements of the standard before and after each sample. The measured sulfur isotopic compositions are reported in delta-notation relative to the international

standard Vienna-Canyon Diablo Troilite (V-CDT):

$$\delta^X\text{S} = 1000 \cdot \left[\frac{(\frac{X}{\text{S}/^{32}\text{S}})_{\text{sample}}}{(\frac{X}{\text{S}/^{32}\text{S}})_{\text{V-CDT}}} - 1 \right], \quad X = 33 \text{ or } 34 \quad (1)$$

3.4. In-house freezing experiment

To evaluate the effects of ice freeze-thaw processes on the distribution of ^{32}S , ^{34}S in meltwater, an in-house freezing experiment was conducted. A 100 mM stock solution of Na_2SO_4 (>99%, Sigma Aldrich) was prepared and diluted to 1 mM. The 1 mM solution was divided into four 50 mL conical tubes and frozen at - 20 °C freezer. Depending on the degrees of frozen (30%, 60%, and 90%), the remaining solution from each tube was recovered to analyze. The entire experiment was repeated 6 times to verify the reliability of the data.

Table 1. Instrument operating conditions for S isotope determination using MC-ICP-MS followed by Moon et al. (2021).

Desolvator setup	
Spray chamber temperature	110°C
Desolvating membrane temperature	160°C
Ar sweep gas	3.3 - 5.5 l/min
N ₂ flow	0.5 - 1.0 l/min
Nebulizer	PFA-100 (ESI)
Flow rate	100 µl/min
Cones	Ni HS1-7 Skimmer cone Ni FB9 Sampler cone
Mass spectrometer and measurement setup	
RF power	1300 W
Cool gas	13.0 l/min
Aux gas	0.8 - 0.6 l/min
Cup configuration	³² S (L4), ³³ S (H1), ³⁴ S (H6)
Resolution mode	Medium resolution (50 µm entrance slit)
Acquisition	50 blocks
Integration time	5 sec
Uptake time	90 sec
Volume of sample	700 µl
Wash + background measurement	14 min

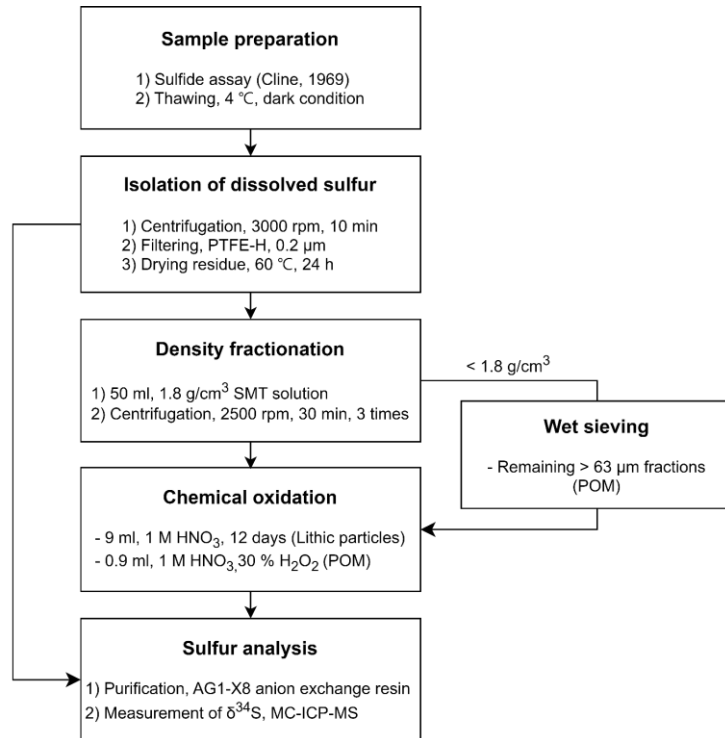


Figure 4. Overall ice wedge sample treatment flow chart for sulfur isotope analysis.

4. Results

Ice wedge samples from 6 sites were analyzed for sulfate concentration and isotopic composition. In some cases, characterized by elevated ice content, the availability of sufficient POM and lithic particles for analysis was limited, solely the liquid components were used. Additionally, for neighboring samples presumed to exhibit similar characteristics in their ice wedges, soil components were combined for comprehensive analysis.

The overall geochemistry data of dissolved sulfate, POM, and lithic particle are shown in Table 2. The mean POM contents measured from the ice wedges is $0.029 \pm 0.021 \text{ g kg}^{-1}$. The minimum value of 0.004 g kg^{-1} was detected in B19-IW10 and the maximum concentration of 0.070 g kg^{-1} in Zy_B-LOW-B. The content of lithic particles ranges from 0.8 g kg^{-1} (Zy_B-LOW-B) to 27.0 g kg^{-1} (B19-IW5), average $9.3 \pm 6.4 \text{ g kg}^{-1}$. The S contents from POM and lithic particles in all samples had approximately similar concentrations. The concentration of dissolved sulfate differed, ranging from $2.7 \text{ }\mu\text{M}$ to $40.9 \text{ }\mu\text{M}$. Within the same ice wedge, the concentration remained relatively stable, except for samples collected in Churapcha, which exhibited a wider range of 3.9 to $40.9 \text{ }\mu\text{M}$. The concentrations for other regions were as follows: Cyuie (2.7 to $9.4 \text{ }\mu\text{M}$), Syrdakh (11.2 to $23.1 \text{ }\mu\text{M}$), Zyryanka (2.21 to $11.51 \text{ }\mu\text{M}$), and Batagay (3.57 to $27.81 \text{ }\mu\text{M}$). The mean sulfur isotopic composition of meltwater ($\delta^{34}\text{S}_{\text{SO}_4}$), POM ($\delta^{34}\text{S}_{\text{POM}}$), and lithic particles ($\delta^{34}\text{S}_{\text{lithic}}$) coincided within an average range of 4‰, with lithic particles generally showing lighter values compared to other components (Figure 5). However, distinct differences were observed between the regions, as Yakutsk

showed enrichment, while Zyryanka and Batagay exhibited relative depletion in a similar manner. Yakutsk, Zyryanka, and Batagay ice wedges showed mean $\delta^{34}\text{S}_{\text{SO}_4}$ of +8.9‰, +1.0‰, and +0.4‰, $\delta^{34}\text{S}_{\text{POM}}$ of +6.8‰, -1.5‰, and +2.0‰, and $\delta^{34}\text{S}_{\text{lithic}}$ of +6.8‰, -1.4‰, and -3.6‰, respectively. In all sampled ice wedges, correlations between concentration and isotope value were generally insignificant (Figure 6).

In the detailed analysis, within the Yakutsk region, Syrdakh exhibited a higher average $\delta^{34}\text{S}_{\text{SO}_4}$ value compared to the Cyuie and Churapcha ice wedges. Churapcha showed a depleted $\delta^{34}\text{S}_{\text{lithic}}$ of approximately 4‰ (Figure 5). The enriched $\delta^{34}\text{S}_{\text{SO}_4}$ and $\delta^{34}\text{S}_{\text{POM}}$ values observed at these three sites closely matched with measurements of +10.4‰ and +9.1‰, respectively, obtained by Chukhrov et al. (1980) from samples collected in modern Central Yakutia during the 1970s. Among the studied sites, Zyryanka was the only location that provided detailed location data within a singular block. This data revealed a discernible trend of concentrated sulfate ions on the side of the ice wedge may influence of permafrost experienced sulfide oxidation or biogeochemical cycle (Figure 7). In the Batagay site, both the upper and lower complexes showed a nearly identical isotopic composition within 1‰. However, a notable distinction was observed that the lower ice complex did not yield any POM in the soil samples used for isotope analysis. Data from Park (2023) revealed that total carbon contents (TOC) ranging from 0.54 wt% to 1.52 wt% and carbon isotope values ($\delta^{13}\text{C}$) in particles from both layers at -25‰, indicating an origin from C3 plant-derived organic carbon. Further examination using scanning electron microscopy (SEM) and energy-dispersive X-ray spectroscopy (EDS) revealed that particles from the Batagay ice wedge were angular rocks characterized by higher density and notable silicon content, ruling

out carbonized organic matter (Figure 8). The TOC and $\delta^{13}\text{C}$ values of these particles (-23.9‰, 1.37 wt%) closely resembled those of the Batagay soil, with TOC content being 1.4 times higher than the mean value.

The results of the in-house freezing experiments are shown in Figure 9. The $\delta^{34}\text{S}$ values were similar to those of the 6 repeated sets of experiments. The sulfate concentration of the remained water was increased from 1 mM to 5 mM in all samples while freezing. The isotope ratios did not change significantly during the phase transition from water to ice; differences between the samples were meaningless within 0.8‰, as reproducibility (2σ) of the $\delta^{34}\text{S}$ analyses ($\pm 0.4\%$) in the same instrument (Moon et al., 2021). As a result of the sulfide assay, all samples showed sulfide concentrations below the 0.2 μm for STD. Therefore, the influence of sulfide oxidation would be negligible.

Table 2. Geochemistry data from the northeastern Siberia.

Sampling sites	Sample ID	dissolved sulfate		Contents (g kg ⁻¹)	POM		Contents (g kg ⁻¹)	Lithic particle		
		Concentration (μM)	δ ³⁴ S (‰)		δ ³⁴ S (‰)	ppm (wt%)		δ ³⁴ S (‰)	ppm (wt%)	
Yakutsk										
Cyuië	CYB03	2.7	8.3	0.052	11.1	1352	6.5	8.9	14	
	CYB04	6.7	9.3	0.019	9.1	4717	5.3	8.0	32	
	CYB05	5.2	8.4	0.064	8.1	4695	18.2	6.7	39	
	CYB06	9.4	8.7	0.018	7.6	2629	7.9	10.1	57	
Churapcha	Chu#2	3.9	8.3	0.018	14.5	5398	6.5	4.7	12	
	Chu#3	21.6	6.5	0.005	11.1	5818	4.1	4.0	40	
	Chu#8	40.7	7.4	0.044	3.3	2713	12.4	4.4	45	
	Chu#9	4.9	9.4				na			
	Chu#16	40.9	7.0	0.045	6.3	3889	11.9	5.3	23	
Syrdakh	SY01	11.2	11.2		na		4.6	7.3	22	
	SY04	23.1	10.3	0.013	6.5	2160	6.1	6.9	28	
	SY07	20.6	11.7	0.016	5.6	2962	4.6	8.3	21	
Zyryanka										
	Zy_A-W1-C	4.7	2.5				na			
	Zy_B-LOW-A	144.1	0.1	0.181	-2.7	6577	198.5	0.7	3	
	Zy_B-LOW-B	4.8	2.2	0.031	-0.8	2765	2.9	-1.4	30	
	Zy_B-LOW-B	11.5	-3.5				na			
	Zy_B-LOW-B	9.9	-1.4	0.070	-1.9	2776	0.8	-1.4	34	

	Zy_B-LOW-B	5.8	3.2	0.005	0.0	3779			
	Zy_B-LOW-C	3.2	1.3				na		
	Zy_B-LOW-D	311.9	3.4	0.371	-1.0	8599	265.3	1.2	2
Batagay									
Upper complex	B19-IW9	11.2	1.6	0.012	0.2	2422	6.1	-2.0	4
	B19-IW10	14.2	2.1	0.004	6.4	2475	16.3	-4.2	4
	B19-IW10	10.2	0.3	0.016	0.9	8796	6.2	-2.3	25
	B19-IW11	3.6	1.3	0.043	1.0	1838	13.7	-4.5	17
	B19-IW11	13.4	-1.3	0.039	1.2	3315	8.7	-4.4	10
Lower complex	B19-IW3	27.8	-0.3				17.1	-5.0	20
	B19-IW5	25.6	-0.8		na		27.0	-2.9	14

Table 3. Sulfur concentration and isotopic composition data from in-house freezing experiment. The experiment was repeated 6 times for accuracy.

Samples	Frozen fraction	Concentration (mM)	$\delta^{34}\text{S}$ (‰)
Exp.1	0.00	1.09	-4.1
	0.35	1.55	-3.8
	0.58	2.14	-4.4
	0.93	4.35	-4.5
Exp.2	0.00	1.12	-4.7
	0.38	1.29	-4.2
	0.66	1.73	-4.3
	0.85	3.29	-4.3
Exp.3	0.00	1.10	-4.0
	0.35	1.65	-4.1
	0.65	2.81	-4.6
	0.96	5.45	-4.3
Exp.4	0.00	1.16	-4.2
	0.28	1.30	-4.1
	0.65	2.81	-4.1
	0.80	6.19	-4.4
Exp.5	0.00	0.83	-4.4
	0.35	1.05	-4.3
	0.58	1.77	-3.8
	0.93	3.55	-4.1
Exp.6	0.00	0.84	-4.5
	0.38	1.05	-4.1
	0.66	1.70	-4.4
	0.85	2.64	-3.9

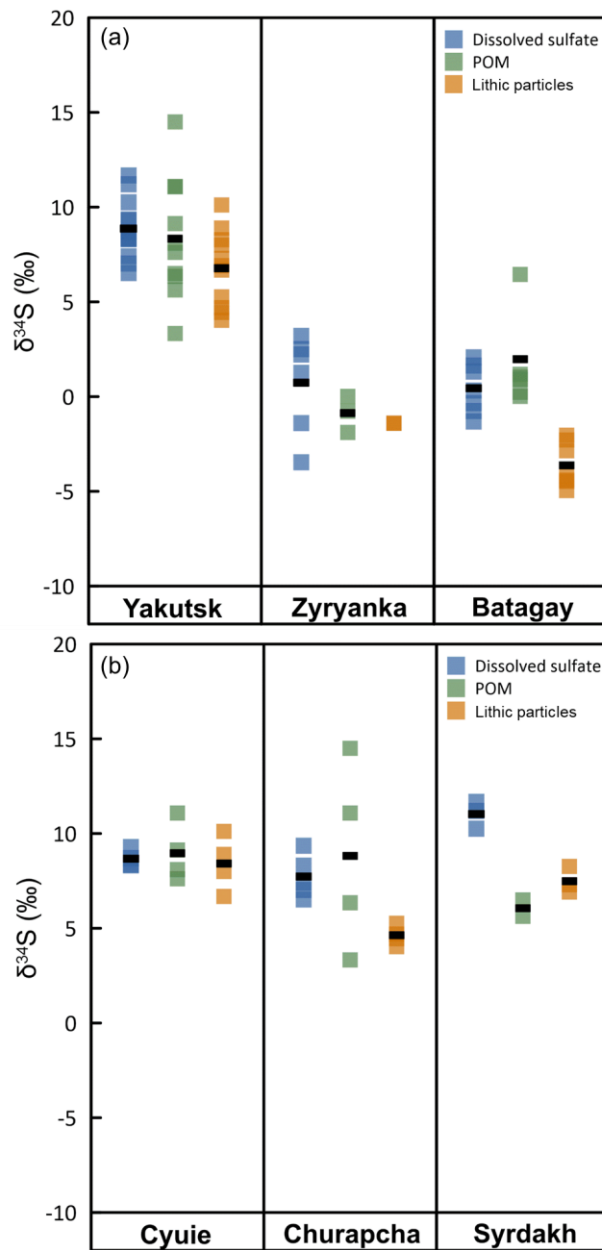


Figure 5. Sulfur isotope values in the ice wedges from the northeastern Siberia used in the study. The black solid square means the average sulfur isotope composition of ice each region. (a) Overall mean sulfur isotope composition of ice wedges from the Yakutsk, Zyryanka and Batagay; (b) Detailed isotope composition of dissolved sulfate, POM, Lithic particles for Yakutsk.

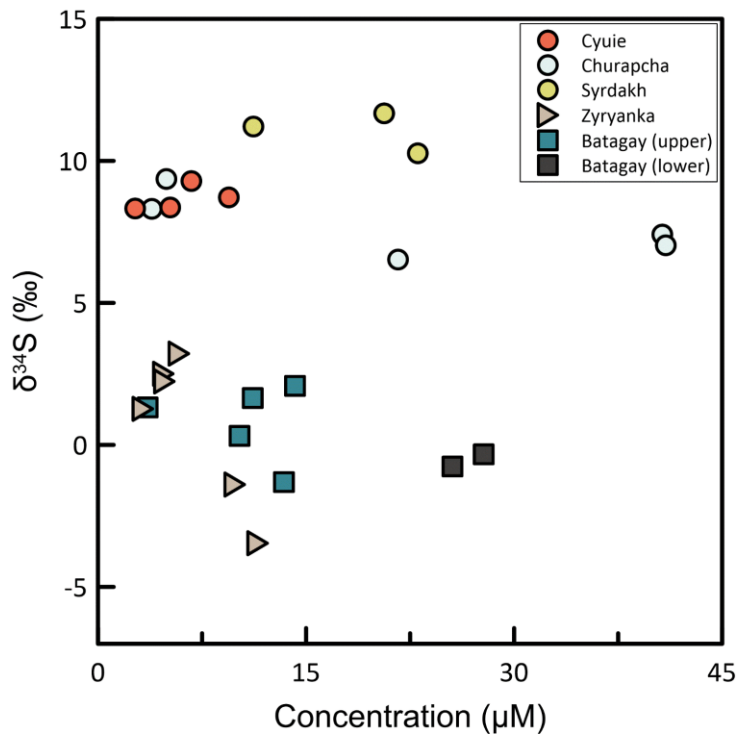


Figure 6. Sulfate concentration and isotope composition of dissolved sulfate in the study area. Dissolved sulfate in the Yakutsk region shows a high sulfur isotopic composition compared to the other two regions.

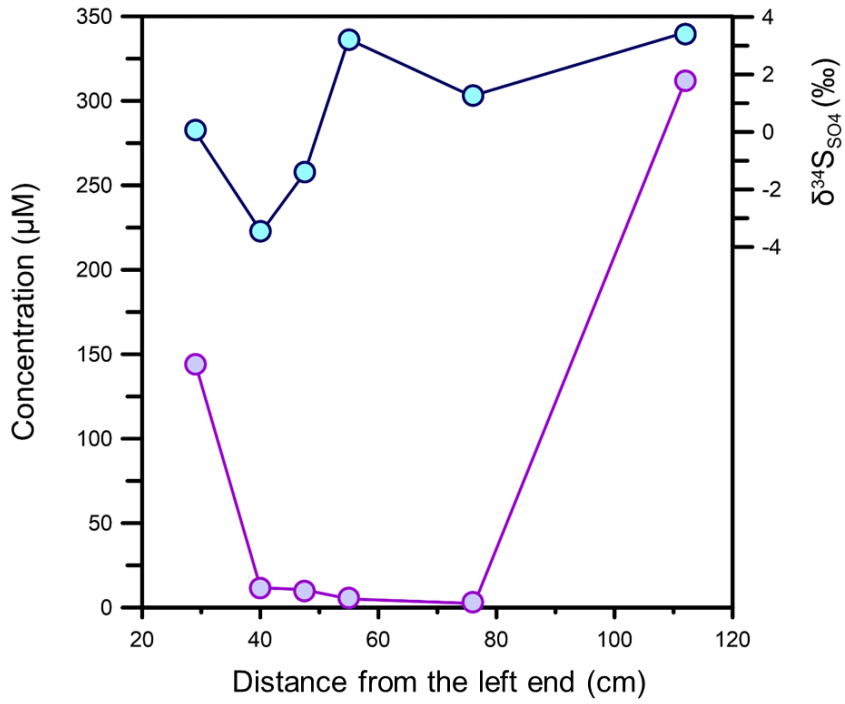


Figure 7. Sulfate concentration and $\delta^{34}\text{S}_{\text{SO}_4}$ within the ice wedge from Zyryanka B site.

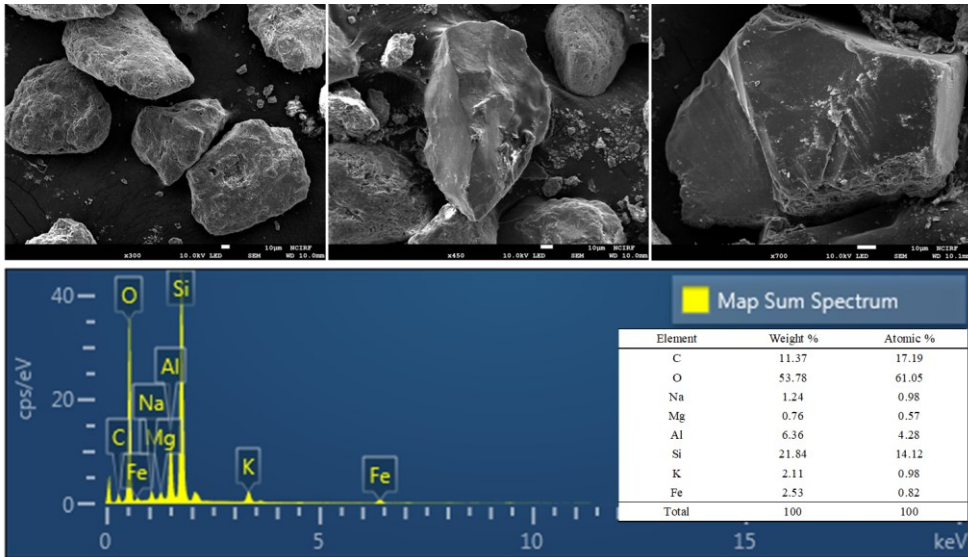


Figure 8. SEM images and EDS elemental spectrum of handpicked sample from B19-IW3 mineral particle. The morphology of the particles and quantification results confirms that the black particles in the Batagay lower ice complex are not of organic origin.

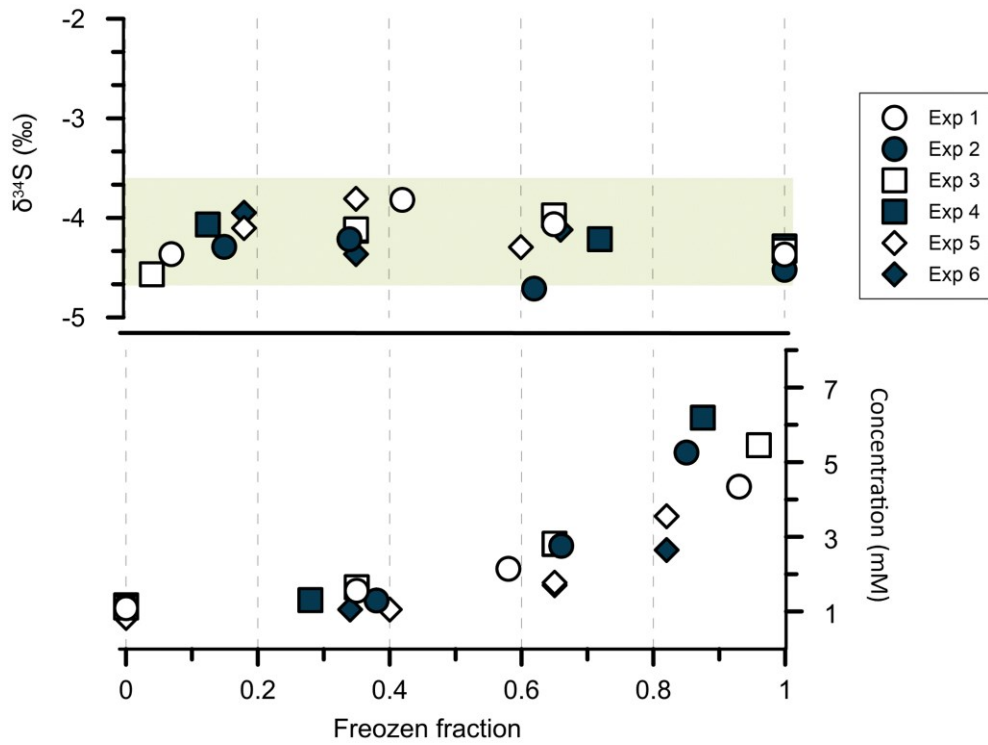


Figure 9. In-house freezing experiment data to evaluate the potential fractionation of $\delta^{34}\text{S}_{\text{SO}_4}$ ($2\sigma = 0.44$).

5. Discussion

5.1. Factors controlling the ice wedge sulfur geochemistry

5.1.1 Dissolved sulfate

The ion chemistry of the ice wedge is influenced by the snow, snow meltwater, and aerosols that accumulate through wet and dry deposition (Iizuka et al., 2019; Holland et al., 2023). Since sulfate behaves nearly conservatively under oxygenated conditions, deposited in the ice wedge would indeed reflect the past atmospheric value (Ohmoto & Lasaga, 1982). The reaction after deposition, especially sulfate reduction by sulfate-reducing bacteria (Sim et al., 2023), however, could alter the source sulfur isotopic composition. When microorganisms utilize sulfate for metabolism in a closed system, sulfide is formed as a product, and sulfate concentrations decrease while the isotopic composition increases. In the study area, all regions show low sulfide levels, and no correlation was observed between changes in sulfate concentrations and isotopic composition (Figure 6). Thus, the occurrence of isotopic fractionation by sulfate-reducing microorganisms is not expected. Along with the observation that the isotopic composition of sulfur remained unchanged during freezing, the findings from the above experiments collectively offer compelling evidence that the ice wedges used in the study effectively preserve the initial sulfate composition, reflecting the aerosol characteristics at its source.

Sulfate in the atmosphere can originate from sea-salt aerosols, biogenic emissions, dust particles, and anthropogenic activities such as fossil-fuel

combustion (Guo et al., 2009). However, in this study, the contribution of anthropogenic sources can be excluded since the youngest ice wedges used was formed at approximately 800 BP (Ko, 2023) before increased human industrial activity. Sea-salt aerosols are one of the largest sources of environmental particles produced by the evaporation of sea spray resulting from breaking waves. The relative contribution of sea-salt (ss) and non-sea-salt (nss) SO_4^{2-} for the dissolved sulfate collected in the ice wedge was estimated according to Keresztesi et al. (2020) based on the ion concentration of Cl^- and SO_4^{2-} in the meltwater. This calculation assumes that a reference element Cl originates exclusively from sea-salt aerosols and that sulfate does not undergo fractionation during aerosol formation or transport. The seawater molar ratio of $\text{SO}_4^{2-}/\text{Cl}^-$ is approximately 0.05 (Zancanaro et al., 2020).

$$\% \text{ ssF} = \frac{100 * [\text{Cl}^-]_{\text{meltwater}} * [\text{SO}_4^{2-}/\text{Cl}^-]_{\text{seawater}}}{[\text{SO}_4^{2-}]_{\text{meltwater}}} \quad (2)$$

$$\% \text{ nssF} = 100 - \text{ssF} \quad (3)$$

The considerable contribution of sea salt, with average percentages of 20%, 39%, and 26% in Yakutsk, Zyryanka, and Batagay, respectively, highlights the significance of considering its impact on the $\delta^{34}\text{S}$ values (Table 4). However, studies investigating the relationship between distance to the coast and $\delta^{34}\text{S}$ have indicated that the sea salt effect is typically limited to distances within 70 km from the coast (Wakshal & Nielsen, 1982), while factors like topography and wind direction can influence this distance (Wadleigh et al., 1994, 1996; Mast et al., 2001). The distance between the three regions in this experiment and the coast is

over 300 km in a straight line, even for the closest region (Batagay). The dominance of $\text{CO}_3^{2-}\text{-Ca}^{2+}$ ions in the Batagay ice wedges also suggests that salts cannot be attributed to marine origins (Vasil'chuck et al., 2020). Instead, the calculated high ssF means that it may be due to contributions from continental salt sources, including stagnant-marsh waters, secondary salts from evaporation and cryogenic mineralization, and brine groundwater, which can be supplied through cracks in the ice (Vasil'chuck, 2016; Alexeev et al., 2020). In addition, the heavy $\delta^{34}\text{S}$ values (+21‰; Ostlund, 1959) of sea-salt compared to the light $\delta^{34}\text{S}$ values (-4.7‰ to +11.7‰) from study sites ruling out that sea-salt is likely a major contributor to dissolved sulfate.

Biogenic emissions pose challenges in explaining the source of sulfate, as the variation of seasonal biogenic activity. Studies of various proxies that can infer biological productivity indicate that marine and terrestrial biological production is more active in summer than winter (Lana et al., 2011; Li et al., 2018). Additionally, volatile biogenic sulfur, which is a product of biological activity, has a relatively short atmospheric lifetime, lasting less than a week (Fischer et al., 2007). Therefore, biogenic sources would have little influence on the $\delta^{34}\text{S}$ values of winter precipitation in northeastern Siberia.

Considering the cold continental climate promoting physical weathering processes at the time of ice wedge formation, lithogenic dust is likely the primary natural source of solutes to the snow. For dust, sulfate can be sourced as evaporite minerals (gypsum, anhydrite, and halite) readily soluble in water and reduced sulfur that undergoes oxidation during weathering. The dissolution of eolian components by precipitation can lead to a shift in the measured $\delta^{34}\text{S}$, potentially

resulting in both higher sourced from evaporite minerals and lower values from reduced sulfur (Wakshal & Nielsen, 1986; Mast et al., 2001; Liebman et al., 2011). Significant dust sources can be attributed to outwash plains during glacial periods, where substantial dust particles were deposited due to glacial abrasion. The glacial ablation led to the removal of surface bedrock, exposing fresh material and increasing the rates of pyrite weathering (Torres et al., 2017). Near the study area, in fact, extensive erosion is believed to have occurred due to glaciation. During the last glacial period and Pleistocene cold stages, the broad expanse of homogeneous loess-like silt originated from the major rivers draining the glaciated terrain and was deposited in valleys with glacial outwash. The wind carried the sediment across outwash plains, depositing silt near Yakutsk and Batagay (Pewe et al., 1983; Ashastina et al., 2017). The loess in the Zyryanka is hypothesized to be a result of the glacially sourced tributaries of the paleo-Kolyma River.

The sulfur isotopes of the three sites exhibit values that are relatively consistent with the geological information in the surrounding area of the study. Central Yakutsk is located on the Siberian Platform, which is extensively covered with sedimentary layers of marine origin, such as marine carbonates, evaporites, continental shelf, and slope sediments (Figure 2; Parfenov, 1991, 1997; Huh et al., 1998). The Siberian evaporite deposited during the Cambrian period shows isotopic compositions reaching up to 30‰ and the presence of sulfide ores from the northwest of the Siberian Platform shows the heavy isotope ^{34}S enrichment (8-11‰; Vinogradov & Grinenko, 1966). In contrast, the bedrock in Zyryanka and Batagay, sourced from the continental tectonic collision zone (Chersky Range, Alazeya-Oloy arc terrane), consists of metamorphosed and volcanic rocks with

slightly lighter $\delta^{34}\text{S}$ values ranging from -5.8‰ to $+2.0\text{‰}$ (Tyukova & Voroshin, 2008; Dubinina et al., 2019), which aligns with the findings of the experiment. Based on the evidence presented, it can be inferred that terrestrial-origin dust had a considerable influence on the sulfur isotopic composition of precipitation.

5.1.2 POM

To plant, sulfur is essential to synthesize essential compounds such as proteins and secondary metabolites (Trust & Fry, 1992), and they obtain sulfur from various sources, including bedrock and natural atmospheric sources, primarily in the form of sulfur dioxide and sulfates (Sparks et al., 2019). During the uptake process, there is negligible fractionation, and any potential fractionation that might occur ($\pm 2\text{‰}$) is considered insignificant compared to the spatial variability in $\delta^{34}\text{S}$ values. So, it is reasonable to expect that pore water and plants would have similar sulfur isotopes. However, biogeochemical processes in the soil, such as sulfate reduction by sulfate-reducing bacteria or oxidation of sulfide, can modify the initial sulfur isotopic composition of the source. Sulfate-reducing bacteria can engender a relatively heavier isotopic signature of sulfate, while the oxidation of sulfide can result in a concomitantly lighter isotopic composition of pore water. Consequently, this isotopically modified sulfate is subsequently assimilated by plants, leading to discernible discrepancies between the source and the plant organic matter in terms of their sulfur isotopic composition. The findings obtained from the sample analysis showed that the average $\delta^{34}\text{S}$ values in dissolved sulfate and POM at the overall regions except for Syrdakh showed no significant differences, but there was only a weak correlation comparing each data. Thus, it is considered that microbial

activity was limited in the vicinity of the ice wedge, and the relatively low $\delta^{34}\text{S}$ values observed at Syrdakh are believed to be a result of the adjacent soil environment, such as sulfide oxidation (Jones et al., 2020), and could also be influenced by the activity of sulfate-oxidizing microorganisms present in nearby wetlands.

Additionally, there was another noteworthy difference in POM content observed between the upper and lower ice complexes of Batagay. The absence of detectable POM was expected to impact TOC and $\delta^{13}\text{C}$ data, but no significant difference was found between the upper and lower layers of the ice wedges analyzed in this study. Previous research has shown that the soil in Batagay was found to contain slate, which can be considered a form of recycled organic matter (Courtin et al., 2022). So, the lower carbon isotope value observed in the lower complex indicates that organic matter could be attributed to recycled carbon, specifically from the slate present in the sample. The narrow, high structural features of the lower ice complex explain the absence of POM in the lower complex in Batagay. Sediments rapidly supplied by neighboring glaciers under the periglacial influence during the formation of the lower ice complex are thought to have disrupted or blocked biological cycling (Shepelev et al., 2018). The vegetation that thrives in the region can impact the amount of organic matter found in the ice wedges. Meadows provide plant species with the highest soil carbon (Wan et al., 2019). As meadows predominantly covered the upper ice complex compared to the lower ice complex (Courtin et al., 2022), they could have supplied more POM than the lower ice complex, where shrubs were more prevalent. Vasil'chuk et al. (2020) also support the environmental change that increased $\delta^{13}\text{C}$

lipids from pedogenic material in ice wedges with depth due to the landscape change from grassland ecosystems to forest ecosystems.

5.1.3 Lithic Particles

Water-soluble sulfate has traditionally been utilized to study aerosol characteristics and origins; however, it is important to recognize that in specific regions, around 50% of total sulfur in dust particles may be insoluble (Huang et al., 2010), indicating that soluble sulfate aerosols only represent a portion of the total dust sources. Consequently, analyzing the insoluble sulfur in ice wedges can yield valuable additional insights into the origin of sulfur deposition. This insoluble sulfur, derived from the reduced form of sulfur with low solubility, offers further information on the sources and processes influencing the sulfur content and isotope in the ice wedges.

At all the studied sites, lithic particles generally showed lighter isotopic compositions compared to dissolved sulfate. The isotopic composition of precipitation is believed to reflect additional sources that can contribute to variations in sulfur isotopes. This finding suggests two potential explanations: 1) the presence of an additional source contributing to the precipitation and 2) the occurrence of fractionation during the oxidation of reduced sulfur. A variety of sulfur sources of precipitation, heavier evaporite like anhydrite (+16.5‰ to +30.2‰ in the Yakutsk; Ryabov et al., 2018) can be present in the atmosphere as fine particles or dissolved in water and directly affect the isotopic composition. These different sulfur sources in the region can contribute to mixing isotopic signatures in precipitation, leading to a range of sulfur isotopic compositions

observed in the northeastern Siberian ice wedge. In addition, in areas of significant physical erosion like glaciated catchments, as the material is removed before reactions are completed, non-stoichiometric stages of pyrite oxidation are expected to occur (Stallard & Edmond, 1983). During pyrite oxidation, in such cases, positive fractionation values ($\epsilon_{\text{SO}_4\text{-sulfide}} = +0.4\text{‰}$ to $+3.5\text{‰}$) can occur (Hindshaw et al., 2016).

5.2. Temporal variation $\delta^{34}\text{S}$ in Ice wedge

In synthesis, the geochemical data acquired from the preceding ice wedges substantiate that modifications in $\delta^{34}\text{S}$ of dissolved sulfate reflect the geological characteristics of the source region and play a crucial role in tracking atmospheric sulfate origins. However, within the scope of this investigation, the sulfur isotopic composition changes were not observed over time. Modern Central Yakutia show enriched $\delta^{34}\text{S}$ of dissolved sulfate, POM ($+10.4\text{‰}$, $+9.1\text{‰}$) each as high as the values during the LGM when the ice wedge formed and two ice complexes in Batagay also exhibit consistent sulfur isotopic values despite a 20 ka time lag, and the time gaps of over 600 ka. The sulfur isotope composition of the Lena and Kolyma rivers, situated near the study region, also has been found to resemble the $\delta^{34}\text{SO}_4$ (Lena River: $+19.3\text{‰}$, Kolyma River: -4.8‰ ; Burke et al., 2018). The bedrock, which is the main sulfate source in the ice wedges, is not easily altered or modified over short periods, as they are influenced by geologic events occurring over long periods of time. These features of the ice wedges can be compared to glaciers, which are already widely used as paleoenvironmental proxies.

Ice core studies, there have already been several reports of $\delta^{34}\text{SO}_4$ changes over

different time timescales (Alexander et al., 2003; Jonsell et al., 2005; Gautier et al., 2018; Burke et al., 2019; Crick et al., 2021). Recently, Uemura et al. (2022) found that in a new record sulfur isotope spanning 6 and 25 kyr BP, LGM to Holocene, the $\delta^{34}\text{SO}_4$ values exhibited a depletion of 3.6‰. These differences are likely due to differences in the types of aerosols that predominantly supply ice wedges and ice core samples. Surrounding thick ice cover nearly all of the continents in polar regions; the influence of surrounding bedrock is limited. Isotopic analyses of Sr and Nd in ice cores from Greenland suggest that the dust mainly originated from sites closer to the edge and at lower altitudes derived from proximal source regions (Bory et al., 2003). This suggests that dust is dominated by local effects when the source is nearby. Instead, long-distance transport of biogenic emissions and terrestrial dust may be the main source of sulfate deposition within the ice sheet (Kaufmann et al., 2010; Goto-Azuma et al., 2019; Fisher et al., 2023). These sources and transport mechanisms of sulfur compounds can be sensitive to fluctuations in climate and environmental conditions, and thus sulfate content and isotopic composition in ice cores reflect changes in atmospheric circulation patterns and ocean productivity (Alexander et al., 2003; Uemura et al., 2022).

However, even in ice wedges that appear uniform on average, variations greater than 5‰ are observed within ice wedges. This variability can be caused by spatial heterogeneity in the underlying rocks or sulfur isotope fractionation during subsurface weathering. Although the overall mean value of bedrock is differentiated between study areas, there are also differences within them: In the study area, the $\delta^{34}\text{S}$ values of sedimentary rocks from the Verkhoyansk-Kolyma fold are significantly lower than those of carbonate and evaporite rocks deposited

in the Siberian crust but vary from -11‰ to +3‰ depending on location and age. Furthermore, sulfide oxidation in anaerobic environments in subglacial environments can enrich the sulfate produced in ^{34}S by up to several ‰ relative to the reactant pyrite (Hindshaw et al., 2016). Consequently, the increased sulfur dust resulting from the preceding glacial abrasion and the resulting pyrite oxidation fractionation is expected to make the concentration and isotopic composition of atmospheric dissolved sulfate sensitive to the glacier system.

Indeed, this study represents the first exploration of sulfur analysis in ice wedges, and many aspects are yet to be investigated and understood. Given the growth of ice wedges over millennia, the $\delta^{34}\text{S}_{\text{SO}_4}$ record contained within them possesses the potential to provide valuable insights into past environmental conditions, including fluctuations in glacial activity within the source region, provided that it can be accurately resolved over an appropriate timescale. However, the limited organic matter content in ice wedge samples presents challenges in conducting high-resolution measurements using carbon isotope analysis with organic matter. Dissolved organic carbon (DOC) dating can be used as an alternative to plant remains for dating ice wedges, providing higher content and uniform distribution compared to plant debris (Wetterich et al., 2023). Therefore, analyzing changes in sulfur isotopic composition through high-resolution precipitation analysis can be a valuable tool for identifying changes within ice wedges.

Table 4. Sea salt contributions of sulfate in ice wedge.

Sampling sites	Sample ID	Concentration (μM)		Sea salt contribution	
		Cl^-	SO_4^{2-}	% _{ssF}	% _{nssF}
Yakutsk					
Cyuie	CYB-04	26.5	2.7	49.4	50.6
	CYB-05	19.9	6.7	14.8	85.2
	CYB-06	44.6	5.2	42.9	57.1
Churapcha	Chu#3	75.8	21.6	17.5	82.5
	Chu#8	58.7	40.7	7.2	92.8
	Chu#16	41.6	40.9	5.1	94.9
Syrdakh	SY01	44.1	11.2	19.7	80.3
	SY04	75.7	23.1	16.4	83.6
	SY07	49.1	20.6	11.9	88.1
Zyryanka					
	Zy_A-W1-C	66.4	4.7	70.4	29.6
	Zy_B-LOW-B	4.8	4.8	5.0	95.0
	Zy_B-LOW-B	78.0	11.5	33.9	66.1
	Zy_B-LOW-B	73.1	9.9	37.1	62.9
	Zy_B-LOW-B	56.4	5.8	48.4	51.6
	Zy_B-LOW-C	167.6	3.2	261.8	-161.8
Batagay					
Upper ice complex	B19-IW9-gas3	94.8	11.2	42.5	57.5
	B19-IW10-gas1	77.7	14.2	27.4	72.6
	B19-IW10-gas2	51.7	10.2	25.4	74.6
	B19-IW11-gas1	72.2	13.4	26.9	73.1
	B19-IW11-gas2	23.5	3.6	32.9	67.1
Lower ice complex	B19-IW3	73.1	27.8	13.1	86.9
	B19-IW5	73.6	25.6	14.4	85.6

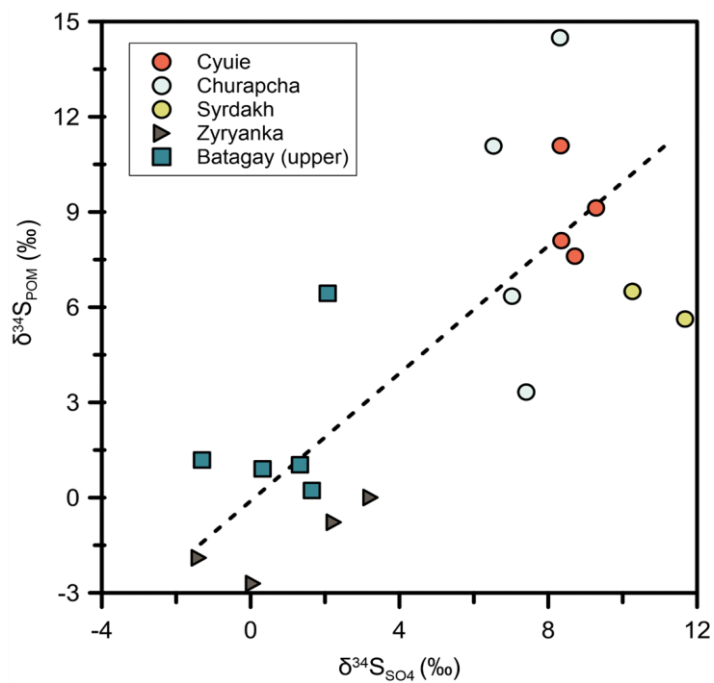


Figure 10. Correlation between $\delta^{34}\text{S}_{\text{SO}_4}$ and $\delta^{34}\text{S}_{\text{POM}}$. Distinct regional trends of heavy and light isotopic compositions are evident in precipitation and organic matter, yet the correlation between these variables appears weak.

6. Conclusion

This study focused on applying sulfur isotope as a proxy to indicate paleoenvironmental conditions in ice wedges and provided valuable insights into the sulfur isotope geochemical data for the first time. To accomplish this objective, sulfur concentrations and isotope compositions of precipitation, POM, and minerals separated from the ice wedge were measured. The study used samples from three locations in Northeast Siberia: Yakutsk, Zyryanka, and Batagay in Russia.

Sulfide concentrations, an indicator of microbial activity in the ice wedge, were measured below the detection limit. Furthermore, the sulfur isotopic composition of precipitation in all three regions tended to be similar to that of POM. This evidence indicates that the sulfur isotopic composition of precipitation in the ice wedge had not undergone further fractionation since the ice wedge formed in the past. Additionally, in-house thawing experiments were conducted to confirm the fractionation of sulfur isotope composition in ice. In-house freezing experiments demonstrated that there was no change in the isotopic distribution when gradually ice frozen.

No significant temporal variations in isotopic composition were detected, while distinct differences in isotopic composition were observed among various bedrock types. All three regions share similar trends in the sulfur isotope composition of dissolved sulfate, POM, and lithic particles, aligning with the sulfur isotopic signature of the local bedrock identified in previous studies. The high sulfur isotopic composition in Yakutsk was attributed to aerosols formed in

exposed evaporites and marine-origin pyrite supplied by enriched sediments. In contrast, the Zyryanka and Batagay relatively light sulfur isotopic composition likely originated from terrestrial origins metamorphosed bedrock.

Sulfur isotopic composition over time shows different behavior in ice wedges and glacier cores. Sulfate composition changes observed exclusively in ice cores on similar time scales indicate the dominant factors influencing the atmospheric sulfur cycle in the study area. During glacial periods, weathering and erosion of nearby bedrock by glacial play a crucial role in influencing the terrestrial sulfur cycle, whereas in polar regions with limited bedrock exposure, long-distance transported biological emission and dust becomes the primary factor. Despite experiencing environmental change or time gap, sulfur isotope composition indicates the source is stable.

However, within the same ice wedge, clear variations in sulfur isotopes were observed, which are thought to be the result of differences in sulfur isotopic composition due to the spatial distribution of bedrock and the effects of fractionation of sulfides by glaciers. The intensity of glacial erosion, which may indicate a transient glacial/interglacial cycle, may indicate that the concentration and isotopic composition of atmospheric dissolved sulfate are expected to be sensitive to the glacier system.

High-resolution age dating within ice wedges is challenging due to insufficient organic matter content, but new methods using DOC are expected to allow comparisons of environmental changes in sulfur over time within ice wedges. Therefore, if it becomes feasible to obtain high-resolution records of sulfate isotope ratios in ice wedges, it is anticipated that differences in $\delta^{34}\text{S}$, linked to diverse rates

of pyrite oxidation, could be observed.

References

- Alexander, B., Thiemens, M., Farquhar, J., Kaufman, A., Savarino, J. *et al.* (2003). East Antarctic ice core sulfur isotope measurements over a complete glacial-interglacial cycle. *Journal of Geophysical Research: Atmospheres*, *108*(D24).
- Alexeev, S., Alexeeva, L., Vakhromeev, A. (2020). Brines of the Siberian platform (Russia): Geochemistry and processing prospects. *Applied Geochemistry*, *117*, 104588.
- Ashastina, K., Schirrmeister, L., Fuchs, M., Kienast, F. (2017). Palaeoclimate characteristics in interior Siberia of MIS 6–2: first insights from the Batagay permafrost mega-thaw slump in the Yana Highlands. *Climate of the Past*, *13*(7), 795-818.
- Bory, A. M., Biscaye, P., Piotrowski, A., Steffensen, J. (2003). Regional variability of ice core dust composition and provenance in Greenland. *Geochemistry, Geophysics, Geosystems*, *4*(12).
- Burke, A., Moore, K. A., Sigl, M., Nita, D. C., McConnell, J. R. *et al.* (2019). Stratospheric eruptions from tropical and extra-tropical volcanoes constrained using high-resolution sulfur isotopes in ice cores. *Earth and Planetary Science Letters*, *521*, 113-119.
- Burke, A., Present, T. M., Paris, G., Rae, E. C., Sandilands, B. H. *et al.* (2018). Sulfur isotopes in rivers: Insights into global weathering budgets, pyrite oxidation, and the modern sulfur cycle. *Earth and Planetary Science Letters*, *496*, 168-177.
- Chukhrov, F., Ermilova, L., Churikov, V., Nosik, L. (1980). The isotopic composition of plant sulfur. *Organic Geochemistry*, *2*(2), 69-75.
- Cline, J. D. (1969). Spectrophotometric determination of hydrogen sulfide in natural waters 1. *Limnology and Oceanography*, *14*(3), 454-458.
- Courtin, J., Perfumo, A., Andreev, A. A., Opel, T., Stoof-Leichsenring, K. R. *et al.* (2022). Pleistocene glacial and interglacial ecosystems inferred from ancient DNA analyses of permafrost sediments from Batagay megaslump, East Siberia. *Environmental DNA*, *4*(6), 1265-1283.

- Craddock, P. R., Rouxel, O. J., Ball, L. A., Bach, W. (2008). Sulfur isotope measurement of sulfate and sulfide by high-resolution MC-ICP-MS. *Chemical geology*, 253(3-4), 102-113.
- Crick, L., Burke, A., Hutchison, W., Kohno, M., Moore, K. A. *et al.* (2021). New insights into the ~ 74 ka Toba eruption from sulfur isotopes of polar ice cores. *Climate of the Past*, 17(5), 2119-2137.
- Donovan, G. H., Jovan, S. E., Gatzolis, D., Burstyn, I., Michael, Y. L. *et al.* (2016). Using an epiphytic moss to identify previously unknown sources of atmospheric cadmium pollution. *Science of the Total Environment*, 559, 84-93.
- Dubinina, E., Filimonova, L., Kossova, S. (2019). Isotope ($\delta^{34}\text{S}$, $\delta^{13}\text{C}$, $\delta^{18}\text{O}$) Compositions of Disseminated Sulfide Mineralization in Igneous Rocks of the Dukat Ore Deposit (Northeastern Russia). *Geology of Ore Deposits*, 61, 38-49.
- Fedorov, A. & Konstantinov, P. (2003). Observations of surface dynamics with thermokarst initiation, Yukechi site, Central Yakutia. Proceedings of the 8th International Conference on Permafrost, 21-25 July 2003, Zurich, Switzerland,
- Fischer, H., Burke, A., Rae, J., Wolff, E., Pryer, H. *et al.* (2023). *Sulfate isotopes over termination II-Source decomposition and Southern Ocean productivity changes.*
- Fischer, H., Siggaard-Andersen, M. L., Ruth, U., Röthlisberger, R., Wolff, E. (2007). Glacial/interglacial changes in mineral dust and sea-salt records in polar ice cores: Sources, transport, and deposition. *Reviews of Geophysics*, 45(1).
- Gautier, E., Savarino, J., Erbland, J., Farquhar, J. (2018). SO₂ oxidation kinetics leave a consistent isotopic imprint on volcanic ice core sulfate. *Journal of Geophysical Research: Atmospheres*, 123(17), 9801-9812.
- Gidrometeoizdat, Leningrad (1989). Handbook on the USSR climate. Series 3. Long-Term Data. Parts 1-6, 24(1), 607 (in Russian)
- Goto-Azuma, K., Hirabayashi, M., Motoyama, H., Miyake, T., Kuramoto, T. *et al.* (2019). Reduced marine phytoplankton sulphur emissions in the Southern

- Ocean during the past seven glacial. *Nature Communications*, 10(1), 3247.
- Guo, Z., Li, Z., Farquhar, J., Kaufman, A. J., Wu, N. *et al.* (2010). Identification of sources and formation processes of atmospheric sulfate by sulfur isotope and scanning electron microscope measurements. *Journal of Geophysical Research: Atmospheres*, 115(D7).
- Hammerli, J., Greber, N. D., Martin, L., Bouvier, A.-S., Kemp, A. I., Fiorentini, M. L., Spangenberg, J. E., Ueno, Y., & Schaltegger, U. (2021). Tracing sulfur sources in the crust via SIMS measurements of sulfur isotopes in apatite. *Chemical geology*, 579, 120242.
- Hannan, K. (1998). Sulfur isotopes in geochemistry. In *Geochemistry* (pp. 610-615).
- Harry, D. G. & Gozdzik, J. S. (1988). Ice wedges: growth, thaw transformation, and palaeoenvironmental significance. *Journal of Quaternary Science*, 3(1), 39-55.
- Hindshaw, R. S., Heaton, T. H., Boyd, E. S., Lindsay, M. R., Tipper, E. T. (2016). Influence of glaciation on mechanisms of mineral weathering in two high Arctic catchments. *Chemical geology*, 420, 37-50.
- Holland, K. M., Porter, T. J., Criscitiello, A. S., Froese, D. G. (2023). Ion geochemistry of a coastal ice wedge in northwestern Canada: Contributions from marine aerosols and implications for ice-wedge paleoclimate interpretations. *Permafrost and Periglacial processes*.
- Huang, K., Zhuang, G., Li, J., Wang, Q., Sun, Y. *et al.* (2010). Mixing of Asian dust with pollution aerosol and the transformation of aerosol components during the dust storm over China in spring 2007. *Journal of Geophysical Research: Atmospheres*, 115(D7).
- Huh, Y., Tsoi, M.-Y., Zaitsev, A., Edmond, J. M. (1998). The fluvial geochemistry of the rivers of Eastern Siberia: I. Tributaries of the Lena River draining the sedimentary platform of the Siberian Craton. *Geochimica et cosmochimica acta*, 62(10), 1657-1676.
- Iizuka, Y., Miyamoto, C., Matoba, S., Iwahana, G., Horiuchi, K. *et al.* (2019). Ion concentrations in ice wedges: An innovative approach to reconstruct past climate variability. *Earth and Planetary Science Letters*, 515, 58-66.

- Ivanova, R. (2003). Seasonal thawing of soils in the Yana River valley, northern Yakutia. Permafrost, proceedings of the eighth international conference on permafrost,
- Jones, E. L., Hodson, A. J., Thornton, S. F., Redeker, K. R., Rogers, J. *et al.* (2020). Biogeochemical processes in the active layer and permafrost of a high Arctic Fjord valley. *Frontiers in Earth Science*, 8, 342.
- Jonsell, U., Hansson, M. E., Mörth, C.-M., Torssander, P. (2005). Sulfur isotopic signals in two shallow ice cores from Dronning Maud Land, Antarctica. *Tellus B: Chemical and Physical Meteorology*, 57(4), 341-350.
- Kaufmann, P., Fundel, F., Fischer, H., Bigler, M., Ruth, U. *et al.* (2010). Ammonium and non-sea salt sulfate in the EPICA ice cores as indicator of biological activity in the Southern Ocean. *Quaternary Science Reviews*, 29(1-2), 313-323.
- Keresztesi, Á., Nita, I.-A., Boga, R., Birsan, M.-V., Bodor, Z. *et al.* (2020). Spatial and long-term analysis of rainwater chemistry over the conterminous United States. *Environmental Research*, 188, 109872.
- Kim, K., Yang, J. W., Yoon, H., Byun, E., Fedorov, A. *et al.* (2019). Greenhouse gas formation in ice wedges at Cyuie, central Yakutia. *Permafrost and Periglacial processes*, 30(1), 48-57.
- Ko, J. (2009). Petroleum Geology of the East Siberian Platform, Russia. *Journal of the Korean Society of Mineral and Energy Resources Engineers*, 46(6), 809-833.
- Ko, N., Park, H., Jung, H., Iwahana, G., Fedorov, A. *et al.* (2022). Understanding formation of ice wedges and origin of trapped greenhouse gas at Zyryanka, Northeastern Siberia. EGU General Assembly Conference Abstracts,
- Ko, N., Yang, J.-W., Iwahana, G., Fedorov, A., Shepelev, A. G. *et al.* (2021). Paleoclimate Inferred from Concentration of Greenhouse Gas and Ratios of O₂/Ar and N₂/Ar in Ice Wedges in Northeastern Siberia and Northern Alaska. EGU General Assembly Conference Abstracts,
- Kunitsky, V., Syromyatnikov, I., Schirrmeister, L., Skachov, Y. B., Grosse, G. *et al.* (2013). Ice-rich permafrost and thermal denudation in the Batagay area (Yana Upland, East Siberia). *Earth Cryosphere (Kriosfera Zemli)*, 17(1),

56-58.

- Lana, A., Bell, T., Simó, R., Vallina, S., Ballabrera-Poy, J. *et al.* (2011). An updated climatology of surface dimethylsulfide concentrations and emission fluxes in the global ocean. *Global biogeochemical cycles*, 25(1).
- Leffingwell, E. d. K. (1915). Ground-ice wedges: The dominant form of ground-ice on the north coast of Alaska. *The Journal of Geology*, 23(7), 635-654.
- Leibman, M., Kizyakov, A., Lein, A. Y., Perednya, D., Savvichev, A. *et al.* (2011). Sulfur and carbon isotopes within atmospheric, surface and ground water, snow and ice as indicators of the origin of tabular ground ice in the Russian Arctic. *Permafrost and Periglacial processes*, 22(1), 39-48.
- Li, J., Michalski, G., Davy, P., Harvey, M., Katzman, T. *et al.* (2018). Investigating source contributions of size-aggregated aerosols collected in Southern Ocean and Baring Head, New Zealand using sulfur isotopes. *Geophysical Research Letters*, 45(8), 3717-3727.
- Mast, M. A., Turk, J. T., Ingersoll, G. P., Clow, D. W., Kester, C. L. (2001). Use of stable sulfur isotopes to identify sources of sulfate in Rocky Mountain snowpacks. *Atmospheric Environment*, 35(19), 3303-3313.
- Meyer, H., Opel, T., Laepple, T., Dereviagin, A. Y., Hoffmann, K. *et al.* (2015). Long-term winter warming trend in the Siberian Arctic during the mid-to late Holocene. *Nature Geoscience*, 8(2), 122-125.
- Meyer, H., Schirmermeister, L., Andreev, A., Wagner, D., Hubberten, H.-W. *et al.* (2010). Lateglacial and Holocene isotopic and environmental history of northern coastal Alaska—Results from a buried ice-wedge system at Barrow. *Quaternary Science Reviews*, 29(27-28), 3720-3735.
- Meyer, H., Schirmermeister, L., Yoshikawa, K., Opel, T., Wetterich, S. *et al.* (2010). Permafrost evidence for severe winter cooling during the Younger Dryas in northern Alaska. *Geophysical Research Letters*, 37(3).
- Murton, J. B., Edwards, M. E., Lozhkin, A. V., Anderson, P. M., Savvinov, G. N. *et al.* (2017). Preliminary paleoenvironmental analysis of permafrost deposits at Batagaika megaslump, Yana Uplands, northeast Siberia. *Quaternary Research*, 87(2), 314-330.
- Murton, J. B., Opel, T., Toms, P., Blinov, A., Fuchs, M. *et al.* (2022). A

- multimethod dating study of ancient permafrost, Batagay megaslump, east Siberia. *Quaternary Research*, 105, 1-22.
- Nehlich, O. (2015). The application of sulphur isotope analyses in archaeological research: a review. *Earth-Science Reviews*, 142, 1-17.
- Nichols, K.&Wright, S. (2006). Carbon and nitrogen in operationally defined soil organic matter pools. *Biology and Fertility of Soils*, 43, 215-220.
- Oduro, H., Van Alstyne, K. L.,Farquhar, J. (2012). Sulfur isotope variability of oceanic DMSP generation and its contributions to marine biogenic sulfur emissions. *Proceedings of the National Academy of Sciences*, 109(23), 9012-9016.
- Ohmoto, H.&Lasaga, A. C. (1982). Kinetics of reactions between aqueous sulfates and sulfides in hydrothermal systems. *Geochimica et cosmochimica acta*, 46(10), 1727-1745.
- Opel, T., Dereviagin, A. Y., Meyer, H., Schirrmeister, L.,Wetterich, S. (2011). Palaeoclimatic information from stable water isotopes of Holocene ice wedges on the Dmitrii Laptev Strait, northeast Siberia, Russia. *Permafrost and Periglacial processes*, 22(1), 84-100.
- Opel, T., Laepple, T., Meyer, H., Dereviagin, A. Y.,Wetterich, S. (2017). Northeast Siberian ice wedges confirm Arctic winter warming over the past two millennia. *The Holocene*, 27(11), 1789-1796.
- Opel, T., Meyer, H., Wetterich, S., Laepple, T., Dereviagin, A. *et al.* (2018). Ice wedges as archives of winter paleoclimate: A review. *Permafrost and Periglacial processes*, 29(3), 199-209.
- Opel, T., Murton, J. B., Wetterich, S., Meyer, H., Ashastina, K. *et al.* (2019). Past climate and continentality inferred from ice wedges at Batagay megaslump in the Northern Hemisphere's most continental region, Yana Highlands, interior Yakutia. *Climate of the Past*, 15(4), 1443-1461.
- Östlund, G. (1959). Isotopic composition of sulfur in precipitation and sea-water. *Tellus*, 11(4), 478-480.
- Panettiere, P., Cortecchi, G., Dinelli, E., Bencini, A., Guidi, M. (2000). Chemistry and sulfur isotopic composition of precipitation at Bologna, Italy. *Applied Geochemistry*, 15(10), 1455-1467.

- Parfenov, L. (1991). Tectonics of the Verkhoyansk-Kolyma Mesozoides in the context of plate tectonics. *Tectonophysics*, 199(2-4), 319-342.
- Parfenov, L. (1997). Geological structure and geological history of Yakutia. *Geological Monuments of the Sakha Republic (Yakutia)*, 61-77.
- Paris, G., Sessions, A. L., Subhas, A. V., Adkins, J. F. (2013). MC-ICP-MS measurement of $\delta^{34}\text{S}$ and $\Delta^{33}\text{S}$ in small amounts of dissolved sulfate. *Chemical geology*, 345, 50-61.
- Park, H., Ko, N.-Y., Kim, J., Opel, T., Meyer, H. *et al.* (2022). Compositions and origins of greenhouse gas species in permafrost ice wedges at the Batagay megaslump, Yana Uplands, Northeast Siberia. EGU General Assembly Conference Abstracts,
- Péwé, T. L. & Journaux, A. (1983). *Origin and character of loesslike silt in unglaciated south-central Yakutia, Siberia, USSR* (2330-7102).
- Popp, S., Diekmann, B., Meyer, H., Siegert, C., Syromyatnikov, I. *et al.* (2006). Palaeoclimate signals as inferred from stable-isotope composition of ground ice in the Verkhoyansk foreland, Central Yakutia. *Permafrost and Periglacial processes*, 17(2), 119-132.
- Ryabov, V., Simonov, O., Snisar, S., Borovikov, A. (2018). The source of sulfur in sulfide deposits in the Siberian Platform traps (from isotope data). *Russian Geology and Geophysics*, 59(8), 945-961.
- Schimmelmann, A. & Kastner, M. (1993). Evolutionary changes over the last 1000 years of reduced sulfur phases and organic carbon in varved sediments of the Santa Barbara Basin, California. *Geochimica et cosmochimica acta*, 57(1), 67-78.
- Shepelev, A. G., Kizyakov, A., Wetterich, S., Cherepanova, A., Fedorov, A. *et al.* (2020). Sub-Surface Carbon Stocks in Northern Taiga Landscapes Exposed in the Batagay Megaslump, Yana Upland, Yakutia. *Land*, 9(9), 305.
- Sim, M. S., Woo, D. K., Kim, B., Jeong, H., Joo, Y. J. *et al.* (2023). What Controls the Sulfur Isotope Fractionation during Dissimilatory Sulfate Reduction? *ACS Environmental Au*, 3(2), 76-86.
- Soare, R., Conway, S., Dohm, J. (2014). Possible ice-wedge polygons and recent

- landscape modification by “wet” periglacial processes in and around the Argyre impact basin, Mars. *Icarus*, 233, 214-228.
- Sparks, J. M., Crowley, B. E., Rutherford, M. G., Jaggernauth, D. (2019). Coastal proximity, orientation, and precipitation amount drive spatial variability in $\delta^{34}\text{S}$ values on the Caribbean island of Trinidad. *Applied Geochemistry*, 108, 104372.
- Stallard, R. & Edmond, J. (1983). Geochemistry of the Amazon: 2. The influence of geology and weathering environment on the dissolved load. *Journal of Geophysical Research: Oceans*, 88(C14), 9671-9688.
- Steiner, B. M. & Barnet, J. S. (2021). Resource potential of one of Earth's final remaining frontiers: the Siberian Platform. *Geology Today*, 37(1), 18-22.
- Thode, H. (1991). Sulphur isotopes in nature and the environment: an overview. *Stable isotopes: natural and anthropogenic sulphur in the environment*, 43, 1-26.
- Torres, M. A., Moosdorf, N., Hartmann, J., Adkins, J. F., West, A. J. (2017). Glacial weathering, sulfide oxidation, and global carbon cycle feedbacks. *Proceedings of the National Academy of Sciences*, 114(33), 8716-8721.
- Trust, B. & Fry, B. (1992). Stable sulphur isotopes in plants: a review. *Plant, Cell & Environment*, 15(9), 1105-1110.
- Tyukova, Y. E. & Voroshin, S. (2008). The sulfur isotopic composition of sulfides from ores and host rocks of the Upper Kolyma region, Magadan Oblast. *Russian Journal of Pacific Geology*, 2, 25-38.
- Uemura, R., Masaka, K., Iizuka, Y., Hirabayashi, M., Matsui, H. *et al.* (2022). Soluble salts in deserts as a source of sulfate aerosols in an Antarctic ice core during the last glacial period. *Earth and Planetary Science Letters*, 578, 117299.
- Vasil'chuk, Y. K. (2016). Geochemical composition of ground ice in the Russian Arctic. *Arctic and Antarctic*, 2, 23-39.
- Vasil'chuk, Y. K., Belik, A., Budantseva, N., Gennadiev, A., Vasil'chuk, J. Y. (2020). Carbon Isotope signatures and polyarenes in the pedogenic material of ice wedges of the Batagay Yedoma (Yakutia). *Eurasian Soil Science*, 53, 187-196.

- Vasil'chuk, Y. K. & Vasil'chuk, J. Y. (2019). The first AMS dating of organic microinclusions in an ice wedge of the upper part of the Batagay yedoma megaslump (Yakutia). *Doklady Earth Sciences*,
- Vasil'chuk, Y. K., Vasil'chuk, J. Y., Budantseva, N., Vasil'chuk, A., Belik, A. *et al.* (2020). Major and trace elements, $\delta^{13}\text{C}$, and polycyclic aromatic hydrocarbons in the Late Pleistocene ice wedges: A case-study of Batagay yedoma, Central Yakutia. *Applied Geochemistry*, 120, 104669.
- Vasil'chuk, Y., Vasil'chuk, J., Budantseva, N., Vasil'chuk, A. (2022). Mis 3–2 Paleo-Winter Temperature Reconstructions Obtained from Stable Water Isotope Records of Radiocarbon-Dated Ice Wedges of the Batagay Ice Complex (yana Upland, Eastern Siberia). *Radiocarbon*, 64(6), 1403-1417.
- Vinogradov, V., Pokrovskiy, B., Pustylnikov, A., Muravyev, V., Shatskiy, G. *et al.* (1994). Isotopno-geokhimicheskie osobennosti i vozrast verkhnedokembriiskikh otlozheniy zapada Sibirskoy platformy. *Litol. Polezn. Iskop*, 4, 49-76.
- Wadleigh, M., Schwarcz, H., Kramer, J. (1994). Sulphur isotope tests of seasalt correction factors in precipitation: Nova Scotia, Canada. *Water, Air, and Soil Pollution*, 77, 1-16.
- Wadleigh, M., Schwarcz, H., Kramer, J. (1996). Isotopic evidence for the origin of sulphate in coastal rain. *Tellus B: Chemical and Physical Meteorology*, 48(1), 44-59.
- Wakshal, E. & Nielsen, H. (1982). Variations of $\delta^{34}\text{S}$ (SO_4), $\delta^{18}\text{O}$ (H_2O) and Cl/SO_4 ratio in rainwater over northern Israel, from the Mediterranean Coast to Jordan Rift Valley and Golan Heights. *Earth and Planetary Science Letters*, 61(2), 272-282.
- Wan, Q., Zhu, G., Guo, H., Zhang, Y., Pan, H. *et al.* (2019). Influence of vegetation coverage and climate environment on soil organic carbon in the Qilian Mountains. *Scientific reports*, 9(1), 17623.
- Wetterich, S., Alexander, I. K., Opel, T., Grotheer, H., Mollenhauer, G. *et al.* (2023). Ground-ice origin and age on Herschel Island (Qikiqtaruk), Yukon, Canada. *Quaternary Science Advances*, 100077.
- Wheal, M. S., Fowles, T. O., Palmer, L. T. (2011). A cost-effective acid digestion

- method using closed polypropylene tubes for inductively coupled plasma optical emission spectrometry (ICP-OES) analysis of plant essential elements. *Analytical Methods*, 3(12), 2854-2863.
- Xiao, H.-Y., Zhu, R.-G., Lin, B.-N., Liu, C.-Q. (2011). Sulfur isotopic signatures in rainwater and moss *Haplocladium microphyllum* indicating atmospheric sulfur sources in Nanchang City (SE China). *Science of the Total Environment*, 409(11), 2127-2132.
- Yang, J. W., Ahn, J., Iwahana, G., Ko, N., Kim, J. H. *et al.* (2023). Origin of CO₂, CH₄, and N₂O trapped in ice wedges in central Yakutia and their relationship. *Permafrost and Periglacial processes*.
- Yang, J.-W., Ahn, J., Iwahana, G., Han, S., Kim, K. *et al.* (2020). Brief Communication: The reliability of gas extraction techniques for analysing CH₄ and N₂O compositions in gas trapped in permafrost ice wedges. *The Cryosphere*, 14(4), 1311-1324.
- Yu, T.-L., Wang, B.-S., Shen, C.-C., Wang, P.-L., Yang, T. F. *et al.* (2017). Improved analytical techniques of sulfur isotopic composition in nanomole quantities by MC-ICP-MS. *Analytica chimica acta*, 988, 34-40.
- Zancanaro, E., Teatini, P., Scudiero, E., Morari, F. (2020). Identification of the Origins of Vadose-Zone Salinity on an Agricultural Site in the Venice Coastland by Ionic Molar Ratio Analysis. *Water*, 12(12), 3363.
- Zhang, M., Wang, S., Ma, G., Zhou, H., Fu, J. (2010). Sulfur isotopic composition and source identification of atmospheric environment in central Zhejiang, China. *Science China Earth Sciences*, 53, 1717-1725.
- 고나연. (2023). *Formation of ice wedges and origin of trapped greenhouse gas at Zyryanka, Northeastern Siberia* 서울대학교 대학원.
- 문종한, 주영지, 강정옥, 심민섭. (2021). Measurement of sulfur isotope ratios in trace amounts of dissolved sulfate by MC-ICP-MS. *지질학회지*, 57(1), 99-108.

국문초록

황은 다양한 생지화학적 반응에 참여하며, 그에 따른 고유한 안정동위원소 비율을 가지기 때문에 고환경 프록시로서 다양한 연구에 이용되고 있다. 최근 얼음썰기는 에어로졸, 강수, 인근 유기물의 저장소로서 평가받으며 고환경 아카이브로서의 역할을 할 수 있을 것으로 알려졌지만, 얼음썰기의 황 동위원소 조성은 종합적으로 탐구되거나 이해된 바가 아직 없다. 본 연구에서는 동시베리아 영구동토층의 얼음썰기를 구성하는 강수, 유기물, 광물질을 대상으로 획득한 황 동위원소 지구화학 자료를 최초로 제공한다. 연구에 이용한 시료는 야쿠츠크 (썬야, 츠랍차, 시르닥), 지르얀카, 바타가이 지역에서 채취하였으며 용존 황산염, 유기물, 광물질로 분리하여 실험을 수행하였다. 지역별 시료의 황 동위원소 조성 값은 용존 황산염, POM, 광물질이 유사한 경향을 보였으며 야쿠츠크는 다른 연구 지역보다 6% 이상 부화되어 보였다. 백 킬로미터 이상 떨어진 야쿠츠크 지역의 썬야, 츠랍차, 시르닥 시료는 서로 유사한 동위원소 조성 값을 가지지만, 바타가이와 지르얀카 지역의 값과 구분되는 연구지역의 기반암과 연관된 것으로 여겨진다. 야쿠츠크 지역의 현생 강수, 식물 황 동위원소 조성과 얼음썰기, 바타가이 상부, 하부의 황 동위원소 조성 비교에서는 시간에 따른 황 동위원소 조성의 차이를 확인할 수 없었다. 반면, 동일 얼음썰기 내에서의 황 동위원소 조성 변화는 모든 연구지역에서 관찰되었는데 이는 황을 포함한 물질의 기원은 안정적으로 유지되지만, 빙하의 발달 정도에 의해 공급되는 물질의 양에는 시간적으로 민감하게 반응할 가능성을 내포하고 있다. 얼음썰기 내에 강수 황 동위원소 조성의 변질 가능성을 확인하기 위해 자체 동결실험 진행과 황화물의 농도 측정을 진행한 결과, 동결 과정과 얼음썰기 내에서 황산염 환원 미생물에 의한 분별 작용은 없었을 것으로 생각되며 얼음썰기에 포함된 황은 기원물질의 동위원소 조성을 보존하고 있음을 나타낸다. 이러한 연구 결과는 황 동위원소 조성이 얼음썰기 형성 당시 주변 환경의 지화학적 정

보를 반영하는 프록시로서의 가능성을 지시하며, 내륙 지역의 얼음썰기에서 기반암이 황 동위원소 구성에 가장 큰 영향을 미치는 요인임을 시사한다. 그뿐만 아니라 최초로 얼음썰기의 황 동위원소 구성을 측정하기 위한 실험적 방법을 정립하고, 결과 값을 제시하여 얼음썰기 형성 환경에 대한 이해를 높이고 시료의 이용 영역을 확장하는 데 기여할 것으로 기대된다.

주제어: 동위원소, 얼음썰기, 암석 풍화, 고기후 프록시, 북동시베리아

학번: 2021-27813